

First-encounter time of two diffusing particles in two- and three-dimensional confinement

F. Le Vot and S. B. Yuste

*Departamento de Física and Instituto de Computación Científica Avanzada (ICCAEx)
Universidad de Extremadura, E-06071 Badajoz, Spain*

E. Abad

*Departamento de Física Aplicada and Instituto de Computación Científica Avanzada (ICCAEx)
Centro Universitario de Mérida
Universidad de Extremadura, E-06800 Mérida, Spain*

D. S. Grebenkov

*Laboratoire de Physique de la Matière Condensée (UMR 7643),
CNRS – Ecole Polytechnique, IP Paris, 91128 Palaiseau, France*

The statistics of the first-encounter time of diffusing particles changes drastically when they are placed under confinement. In the present work, we make use of Monte Carlo simulations to study the behavior of a two-particle system in two- and three-dimensional domains with reflecting boundaries. Based on the outcome of the simulations, we give a comprehensive overview of the behavior of the survival probability $S(t)$ and the associated first-encounter time probability density $H(t)$ over a broad time range spanning several decades. In addition, we provide numerical estimates and empirical formulas for the mean first-encounter time $\langle T \rangle$, as well as for the decay time T characterizing the monoexponential long-time decay of the survival probability. Based on the distance between the boundary and the center of mass of two particles, we obtain an empirical lower bound t_B for the time at which $S(t)$ starts to significantly deviate from its counterpart for the no boundary case. Surprisingly, for small-sized particles, the dominant contribution to T depends only on the total diffusivity $D = D_1 + D_2$, in sharp contrast to the one-dimensional case. This contribution can be related to the Wiener sausage generated by a fictitious Brownian particle with diffusivity D . In two dimensions, the first subleading contribution to T is found to depend weakly on the ratio D_1/D_2 . We also investigate the slow-diffusion limit when $D_2 \ll D_1$ and discuss the transition to the limit when one particle is a fixed target. Finally, we give some indications to anticipate when T can be expected to be a good approximation for $\langle T \rangle$.

PACS numbers: 02.50.-r, 05.40.-a, 02.70.Rr, 05.10.Gg

Keywords: First-passage time, First-encounter time, Diffusion-influenced reactions

I. INTRODUCTION

The first-encounter time (FET) of diffusing particles is one of the central quantities characterizing diffusion-influenced reactions. Smoluchowski first recognized the importance of the encounter step by showing that the bimolecular reaction rate of two spherical particles is proportional to their linear sizes and diffusivities [1]. The original problem of two particles diffusing in the three-dimensional Euclidean space is equivalent here to the simpler problem of a single particle diffusing towards a static target. Smoluchowski solved the single-particle diffusion equation and determined the survival probability and thus the probability density of the first-passage time to the target, which is here equivalent to the FET. Since his seminal work, first-passage times to static targets have been thoroughly investigated for various kinds of diffusion processes, chemical kinetics, and geometric settings [2–27]. In the case of a fixed small target embedded in an otherwise reflecting boundary, one deals with the so-called narrow escape problem, for which many asymptotic results have been derived [28–37] (see also a review

[38]). Numerous studies were also dedicated to the problem of multiple particles diffusing on translationally invariant (both finite and infinite) lattices or in Euclidean spaces, which is relevant to chemical reactions involving various species (see [39–46] and references therein). In particular, the effect of inter-particle interactions (e.g., excluded volume), and the cooperativity effect when, for instance, several predators hunt for a prey, were analyzed [47–53]. Theoretical developments have been complemented by numerical approaches, in which diffusion-reaction processes were modeled by molecular dynamics or Monte Carlo simulations [54–56].

In spite of this progress, the statistics of the FET between two particles diffusing in confined domains remains poorly understood. As the translational symmetry is broken by the presence of a confining boundary, the reduction of two diffusing particles to a single particle diffusing towards a static target is prohibited. One has therefore to describe the dynamics of two particles inside a confining domain, and the solution of diffusion-reaction equations becomes much more sophisticated. Amitai *et al.* estimated the mean first-encounter time (MFET) between two ends of a polymer chain by computing the

mean time for a Brownian particle to reach a narrow domain in the polymer configuration space [57]. Tzou *et al.* studied the MFET for two particles diffusing on a one-dimensional interval by solving the underlying diffusion equations [58]. In particular, they discussed the question whether a mobile trap can improve capture times over a fixed trap. Even for such a simple geometric setting, an analytical solution of the problem was not provided. Agliari *et al.* investigated the encounter problem for random walks on branched structures, in particular, on combs [59–61]. More recently, Lawley and Miles computed the MFET for a very general diffusion model with many *small* targets that can diffuse either inside a three-dimensional domain, or on its two-dimensional boundary, their diffusivities can stochastically fluctuate, while their reactivity can be stochastically gated [62]. Nayak *et al.* investigated the capture of a diffusive prey by multiple predators in confined space via intensive Monte Carlo simulations [63]. In particular, they focused on the characteristic timescale associated with rare capture events and its dependence on the number of searchers, the relative diffusivity of the target with respect to the searcher, and the system size. In our former paper [64], we brought some analytic insights into the influence of confinement onto the distribution of the FET in one-dimensional settings, namely, for two particles diffusing on the half-line or on an interval. As discussed below, the problem of two particles could be mapped here onto an equivalent problem of a single particle diffusing on a planar region (a wedge or a rectangle) and then solved exactly.

In this companion paper, we extend our analysis to two- and three-dimensional confining domains. We consider two Brownian particles *A* and *B* diffusing inside a bounded domain with reflecting boundary, until their encounter that triggers an instantaneous chemical reaction: $A + B \rightarrow C$. We investigate the survival probability, i.e., the probability of both particles not having met up to a given time t . The survival probability can be interpreted as the fraction of particles still reactive at time t with respect to the initial number of particles, and it determines other important quantities such as the probability density of the FET (whence its mean value and higher order moments follow, as well as the reaction rate).

The paper is organized as follows. In Sec. II, we formulate the diffusion-reaction problem and summarize the main known theoretical results that are relevant for our study. The Monte Carlo simulations and the statistical tools for analysis of the survival probability and the FET probability density for two particles inside a disk and a sphere with reflecting boundary are described in Sec. III. The analysis in two dimensions is developed for the particular case of a single particle in the search for a fixed target (Sec. IV), for two identical diffusing particles (Sec. V), and for two particles with different diffusivities (Sec. VI). Extensions to the three-dimensional case are presented in Sec. VII, while the main conclusions are summarized in Sec. VIII. The appendix describes the details of Monte Carlo simulations.

II. SUMMARY OF SOME KNOWN THEORETICAL RESULTS

In this section, we summarize some theoretical results on the first-encounter time in two- and three-dimensional space. Even though these results are known, they are dispersed in the literature and not easily accessible. A summary of results for one-dimensional settings was provided in [64].

A. Two diffusing particles

We consider two spherical particles of radii ρ_1 and ρ_2 , started from prescribed points \mathbf{x}_1 and \mathbf{x}_2 and diffusing with diffusion coefficients D_1 and D_2 in a d -dimensional Euclidean domain $\Omega \subset \mathbb{R}^d$ with a smooth reflecting boundary $\partial\Omega$. The first-encounter time \mathcal{T} of these particles is a random variable characterized by the cumulative probability distribution, $\mathbb{P}\{\mathcal{T} < t\}$, or, equivalently, by the survival probability $S(t|\mathbf{x}_1, \mathbf{x}_2) = \mathbb{P}\{\mathcal{T} > t\}$. As the encounter depends on positions of both particles, it is natural to consider their joint dynamics in the phase space $\Omega \times \Omega$, which is governed by the second-order differential operator

$$\mathcal{D} = -(D_1\Delta_{\mathbf{x}_1} + D_2\Delta_{\mathbf{x}_2}), \quad (1)$$

where $\Delta_{\mathbf{x}_i}$ is the Laplace operator acting on \mathbf{x}_i . The survival probability satisfies the joint diffusion equation:

$$\frac{\partial S}{\partial t} = -\mathcal{D}S \quad (\mathbf{x}_1, \mathbf{x}_2) \in \Omega \times \Omega, \quad (2)$$

subject to the initial condition $S(t=0|\mathbf{x}_1, \mathbf{x}_2) = 1$. As the boundary $\partial\Omega$ of the confining domain Ω is reflecting (there is no net diffusive flux across the boundary), the Neumann boundary condition applies for both particles:

$$\frac{\partial S}{\partial n_1} = 0 \quad (\mathbf{x}_1, \mathbf{x}_2) \in \partial\Omega \times \Omega, \quad (3a)$$

$$\frac{\partial S}{\partial n_2} = 0 \quad (\mathbf{x}_1, \mathbf{x}_2) \in \Omega \times \partial\Omega, \quad (3b)$$

where $\partial/\partial n_i$ is the normal derivative at the boundary point \mathbf{x}_i oriented outward Ω . As we are interested in the first encounter, the Dirichlet boundary condition is imposed whenever the particles are at contact, i.e., within the distance $|\mathbf{x}_1 - \mathbf{x}_2| = \rho$:

$$S = 0 \quad (\mathbf{x}_1, \mathbf{x}_2) \in \Gamma, \quad (4)$$

where $\Gamma = \{(\mathbf{x}_1, \mathbf{x}_2) \in \Omega \times \Omega : |\mathbf{x}_1 - \mathbf{x}_2| = \rho\}$, with

$$\rho = \rho_1 + \rho_2. \quad (5)$$

In other words, the first-encounter time of two diffusing particles is equivalent to the first-passage time of a single diffusive process $(X_t^{(1)}, X_t^{(2)})$, describing the motion of

these particles, to the target Γ . The survival probability determines the probability density of the FET,

$$H(t|\mathbf{x}_1, \mathbf{x}_2) = -\frac{\partial S(t|\mathbf{x}_1, \mathbf{x}_2)}{\partial t}, \quad (6)$$

as well as the moments (if they exist):

$$\langle \mathcal{T}^k \rangle = \int_0^\infty dt t^k H(t|\mathbf{x}_1, \mathbf{x}_2) = k \int_0^\infty dt t^{k-1} S(t|\mathbf{x}_1, \mathbf{x}_2), \quad (7)$$

with $k = 1, 2, \dots$. In particular, the MFET is the area below the survival probability curve:

$$\langle \mathcal{T} \rangle = \int_0^\infty dt S(t|\mathbf{x}_1, \mathbf{x}_2). \quad (8)$$

From Eqs. (2)-(4) and Eq. (7), one also finds that the moments $\langle \mathcal{T}^k \rangle$ (if they exist) satisfy the well-known hierarchy of PDEs

$$\mathcal{D}\langle \mathcal{T}^k \rangle = k\langle \mathcal{T}^{k-1} \rangle \quad (\mathbf{x}_1, \mathbf{x}_2) \in \Omega \times \Omega, \quad (9)$$

with

$$\frac{\partial \langle \mathcal{T}^k \rangle}{\partial n_1} = 0 \quad (\mathbf{x}_1, \mathbf{x}_2) \in \partial\Omega \times \Omega, \quad (10a)$$

$$\frac{\partial \langle \mathcal{T}^k \rangle}{\partial n_2} = 0 \quad (\mathbf{x}_1, \mathbf{x}_2) \in \Omega \times \partial\Omega, \quad (10b)$$

and

$$\langle \mathcal{T}^k \rangle = 0 \quad (\mathbf{x}_1, \mathbf{x}_2) \in \Gamma. \quad (11)$$

For any *bounded* domain Ω , the solution of the boundary value problem (2) – (4) can be formally expanded over the eigenfunctions of the governing diffusion operator \mathcal{D} in Eq. (2):

$$S(t|\mathbf{x}_1, \mathbf{x}_2) = \sum_{n=1}^{\infty} e^{-\Lambda_n t} U_n(\mathbf{x}_1, \mathbf{x}_2) \int_{\Omega \times \Omega} d\mathbf{x}'_1 d\mathbf{x}'_2 U_n^*(\mathbf{x}'_1, \mathbf{x}'_2), \quad (12)$$

where the asterisk denotes the complex conjugate, Λ_n are the eigenvalues and $U_n(\mathbf{x}_1, \mathbf{x}_2)$ are the $L_2(\Omega \times \Omega)$ -normalized eigenfunctions of \mathcal{D} : $\mathcal{D}U_n = \Lambda_n U_n$ ($n = 1, 2, \dots$) [65]. The eigenvalues are positive, have units of inverse time, and can be enumerated in the ascending order: $0 \leq \Lambda_1 \leq \Lambda_2 \leq \dots \nearrow +\infty$, whereas the eigenfunctions form a complete basis allowing for such spectral expansions. In particular, the survival probability and the FET density exhibit an exponential decay at long times,

$$S(t|\mathbf{x}_1, \mathbf{x}_2) \propto e^{-t/T} \quad (t \rightarrow \infty), \quad (13)$$

with the decay time

$$T = \frac{1}{\Lambda_1}, \quad (14)$$

determined by the smallest eigenvalue Λ_1 . We emphasize that T does not depend on the starting points \mathbf{x}_1 and \mathbf{x}_2 . The exponential decay implies that all positive moments of \mathcal{T} are finite.

In the previous paper [64], we discussed how this general description can be applied in one-dimensional settings, in which $\Omega \times \Omega$ is a planar region and Γ is either a half-line or an interval. In higher dimensions ($d \geq 2$), Γ is a $(2d - 1)$ -dimensional region (of nontrivial shape) in a $2d$ -dimensional domain $\Omega \times \Omega$ that makes analytical solutions generally unfeasible. An exception is the case of diffusion in free space, $\Omega = \mathbb{R}^d$, for which the change of coordinates simplifies the problem and allows one to get the solution:

(i) In three dimensions, the solution was found by Smoluchowski [1],

$$S_{\text{free}}(t|\mathbf{x}_1, \mathbf{x}_2) = 1 - \frac{\rho}{r} \operatorname{erfc}\left(\frac{r - \rho}{\sqrt{4Dt}}\right), \quad (15)$$

where

$$r = |\mathbf{x}_1 - \mathbf{x}_2|$$

is the initial distance between the centers of two particles,

$$D = D_1 + D_2, \quad (16)$$

and $\operatorname{erfc}(z)$ is the complementary error function. The probability density of the FET is

$$H_{\text{free}}(t|\mathbf{x}_1, \mathbf{x}_2) = \frac{\rho}{r} \frac{r - \rho}{\sqrt{4\pi Dt^3}} \exp\left(-\frac{(r - \rho)^2}{4Dt}\right). \quad (17)$$

(ii) In two dimensions, there is an explicit formula for the Laplace transform of the survival probability:

$$\begin{aligned} \tilde{S}_{\text{free}}(p|\mathbf{x}_1, \mathbf{x}_2) &= \int_0^\infty dt e^{-pt} S_{\text{free}}(t|r) \\ &= \frac{1}{p} \left(1 - \frac{K_0(r\sqrt{p/D})}{K_0(\rho\sqrt{p/D})}\right), \end{aligned} \quad (18)$$

where $K_\nu(\cdot)$ is the ν th-order modified Bessel function of the second kind. The inverse Laplace transform can be expressed as [36]

$$\begin{aligned} S_{\text{free}}(t|\mathbf{x}_1, \mathbf{x}_2) &= \frac{2}{\pi} \int_0^\infty \frac{dq}{q} e^{-Dtq^2} \\ &\times \frac{Y_0(qr)J_0(q\rho) - J_0(qr)Y_0(q\rho)}{J_0^2(q\rho) + Y_0^2(q\rho)}, \end{aligned} \quad (19)$$

where $J_\nu(\cdot)$ and $Y_\nu(\cdot)$ are respectively the ν th-order Bessel functions of the first and second kind. One also gets

$$\begin{aligned} H_{\text{free}}(t|\mathbf{x}_1, \mathbf{x}_2) &= \frac{2D}{\pi} \int_0^\infty dq q e^{-Dtq^2} \\ &\times \frac{Y_0(qr)J_0(q\rho) - J_0(qr)Y_0(q\rho)}{J_0^2(q\rho) + Y_0^2(q\rho)}. \end{aligned} \quad (20)$$

This integral representation allows for a rapid numerical computation of $H_{\text{free}}(t|\mathbf{x}_1, \mathbf{x}_2)$. Levitz *et al.* proposed an explicit approximation for this density [66], but it is only valid when r is close to ρ (see the discussion in the Supplemental Information of [36]). This density exhibits an extremely slow decay at long times:

$$H_{\text{free}}(t|\mathbf{x}_1, \mathbf{x}_2) \simeq \frac{2(r/\rho - 1)}{t \ln^2(2Dt/\rho^2)} \quad (t \rightarrow \infty), \quad (21)$$

as well as the survival probability:

$$S_{\text{free}}(t|\mathbf{x}_1, \mathbf{x}_2) \simeq \frac{2(r/\rho - 1)}{\ln(2Dt/\rho^2)} \quad (t \rightarrow \infty). \quad (22)$$

B. Single particle diffusing towards a static target

Due to mathematical challenges encountered in the analysis of the above problem (2)-(4) for two diffusing particles in a confinement, most former theoretical works dealt with a much simpler setting, in which one particle diffuses towards an immobile particle considered as a static target or a sink [2-26]. This problem is equivalent to diffusion of a single point-like particle with diffusivity $D_1 = D$ inside a modified domain Ω' :

$$\Omega' = \{\mathbf{x}_1 \in \Omega : |\mathbf{x}_1 - \partial\Omega| > \rho_1, |\mathbf{x}_1 - \mathbf{x}_2| > \rho\}, \quad (23)$$

where \mathbf{x}_2 is the fixed position of the target (i.e., the second particle with diffusivity $D_2 = 0$), and $|\mathbf{x}_1 - \partial\Omega|$ is the Euclidean distance from \mathbf{x}_1 to the boundary $\partial\Omega$. In other words, the diffusing particle of radius ρ_1 cannot get closer to the boundary $\partial\Omega$ of the confining domain Ω than by a distance ρ_1 , and cannot overlap with the fixed target of radius ρ_2 . The survival probability satisfies the ordinary diffusion equation,

$$\frac{\partial S}{\partial t} = D\Delta_{\mathbf{x}_1} S \quad \mathbf{x}_1 \in \Omega', \quad (24)$$

subject to the initial condition $S(t=0|\mathbf{x}_1) = 1$ and the mixed boundary conditions:

$$\frac{\partial S}{\partial n} = 0 \quad \mathbf{x}_1 \in \partial\Omega', \quad (25)$$

$$S = 0 \quad \mathbf{x}_1 \in \Gamma', \quad (26)$$

where $\partial\Omega' = \{\mathbf{x}_1 \in \Omega : |\mathbf{x}_1 - \partial\Omega| = \rho_1\}$ is the reflecting boundary of the shrunk confining domain Ω' , and $\Gamma' = \{\mathbf{x}_1 \in \Omega : |\mathbf{x}_1 - \mathbf{x}_2| = \rho\}$ is the encounter region (for the sake of simplicity, we assumed that $|\mathbf{x}_2 - \partial\Omega| > \rho$, i.e. $\partial\Omega'$ and Γ' are disjoint; but more general settings can be considered as well).

As the boundary value problem (24 – 26) has been thoroughly investigated and reviewed in the past, we only summarize several results that will be relevant for our analysis. For any bounded domain Ω' , the spectrum of

the Laplace operator is discrete, and the solution of (24, 25) admits a general spectral expansion [4, 65]

$$S(t|\mathbf{x}_1, \mathbf{x}_2) = \sum_{n=1}^{\infty} u_n(\mathbf{x}_1; \mathbf{x}_2) e^{-t\lambda_n(\mathbf{x}_2)} \int_{\Omega'} d\mathbf{x}' u_n^*(\mathbf{x}'; \mathbf{x}_2), \quad (27)$$

where λ_n and u_n are the n th eigenvalue and $L_2(\Omega')$ -normalized eigenfunction of the diffusion operator $\mathcal{D}' = -D\Delta_{\mathbf{x}_1}$, both depending on the position \mathbf{x}_2 of the static target through the shape of Ω' . To avoid confusion, we distinguish the eigenpairs (λ_n, u_n) from (Λ_n, U_n) used in the case of two diffusing particles. The eigenvalues can be ordered such as $0 < \lambda_1 \leq \lambda_2 \leq \dots \nearrow +\infty$. In particular, the survival probability decays exponentially at long times,

$$S(t|\mathbf{x}_1, \mathbf{x}_2) \propto e^{-t/T(\mathbf{x}_2)} \quad (t \rightarrow \infty), \quad (28)$$

with the decay time $T(\mathbf{x}_2)$ determined by the smallest eigenvalue:

$$T(\mathbf{x}_2) = \frac{1}{\lambda_1(\mathbf{x}_2)}, \quad (29)$$

where we highlighted the dependence on the target position \mathbf{x}_2 , in contrast to the case (14) of two diffusing particles.

Concentric domains

The eigenvalues and eigenfunctions of the diffusion operator are in general not known explicitly. One of few exceptions is the case when Γ and $\partial\Omega$ are concentric circles or spheres of radii ρ and R , respectively (i.e., $\mathbf{x}_2 = 0$). In this case, the rotational symmetry of Ω' implies that $S(t|\mathbf{x}_1, \mathbf{x}_2)$ depends on \mathbf{x}_1 only via its radial coordinate, $r = |\mathbf{x}_1 - \mathbf{x}_2| = |\mathbf{x}_1|$, that allows one to solve Eq. (24) in the Laplace space [4] (see also [66–68]). Denoting by \tilde{S} and \tilde{H} the Laplace transforms of S and H , respectively, the solution can be written as

$$\tilde{S}(p|\mathbf{x}_1, \mathbf{x}_2) = \frac{1}{p} \left[1 - \tilde{H}(p|\mathbf{x}_1, \mathbf{x}_2) \right], \quad (30)$$

with

$$\tilde{H}(p|\mathbf{x}_1, \mathbf{x}_2) = (\rho/r)^\nu \frac{I_{\nu+1}(z\bar{R})K_\nu(zr) + K_{\nu+1}(z\bar{R})I_\nu(zr)}{I_{\nu+1}(z\bar{R})K_\nu(z\rho) + K_{\nu+1}(z\bar{R})I_\nu(z\rho)}, \quad (31)$$

where $\nu = d/2 - 1$, $z = \sqrt{p/D}$, $I_\nu(\cdot)$ is the ν th-order modified Bessel function of the first kind, and

$$\bar{R} = R - \rho_1.$$

More explicitly, one has

$$\tilde{H}(p|\mathbf{x}_1, \mathbf{x}_2) = \frac{I_1(z\bar{R})K_0(zr) + K_1(z\bar{R})I_0(zr)}{I_1(z\bar{R})K_0(z\rho) + K_1(z\bar{R})I_0(z\rho)} \quad (32)$$

in two dimensions, and

$$\tilde{H}(p|\mathbf{x}_1, \mathbf{x}_2) = \frac{\rho}{r} \frac{\bar{R}z \cosh(\bar{R}-r)z - \sinh(\bar{R}-r)z}{\bar{R}z \cosh(\bar{R}-\rho)z - \sinh(\bar{R}-\rho)z} \quad (33)$$

in three dimensions.

The inverse Laplace transform of $\tilde{H}(p|\mathbf{x}_1, \mathbf{x}_2)$ can be performed by means of the residue theorem. These expressions determine all the moments of the FET, in particular,

$$\langle \mathcal{T} \rangle = \frac{\bar{R}^2 \ln(r/\rho)}{2D} - \frac{r^2 - \rho^2}{4D} \quad (d=2), \quad (34)$$

$$\langle \mathcal{T} \rangle = \frac{\bar{R}^3(r-\rho)}{3Dr\rho} - \frac{r^2 - \rho^2}{6D} \quad (d=3). \quad (35)$$

The eigenvalues λ_n contributing to the survival probability and to the FET probability density are related to the poles of Eqs. (32, 33):

$$\lambda_n = \alpha_n^2 / \bar{R}^2, \quad (36)$$

where α_n are positive solutions of

$$J_1(\alpha_n)Y_0(\alpha_n\rho/\bar{R}) - Y_1(\alpha_n)J_0(\alpha_n\rho/\bar{R}) = 0 \quad (37)$$

in two dimensions, and of

$$\tan[\alpha_n(1 - \rho/\bar{R})] = \alpha_n \quad (38)$$

in three dimensions. In the small target limit, $\rho \rightarrow 0$, the smallest eigenvalue λ_1 vanishes as:

$$\lambda_1 \simeq \frac{D}{\bar{R}^2} \begin{cases} 2/\ln(\bar{R}/\rho) & (d=2), \\ 3\rho/\bar{R} & (d=3), \end{cases} \quad (39)$$

so that the decay time T from Eq. (29) increases as

$$T \simeq \frac{\bar{R}^2}{Dd} \begin{cases} \ln(\bar{R}/\rho) & (d=2), \\ \bar{R}/\rho & (d=3) \end{cases} \quad (40)$$

in the leading order. It is instructive to compare the time T with the mean first-passage time (MFPT) $\langle \mathcal{T} \rangle$ given by Eqs. (34), (35):

$$\frac{2dD}{\bar{R}^2}(T - \langle \mathcal{T} \rangle) \simeq \begin{cases} 2\ln(\bar{R}/r) + (r/\bar{R})^2 & (d=2), \\ 2(\bar{R}/r) + (r/\bar{R})^2 & (d=3). \end{cases} \quad (41)$$

One sees that the decay time T always exceeds $\langle \mathcal{T} \rangle$, and that the difference between these two quantities is minimal at $r = \bar{R}$. This is a signature of the prevalence of long trajectories in the behavior of the long time decay; note that the MFET may be smaller *or* larger than the decay time in the case of two diffusing particles (see Sec. VI).

In the limit $R \rightarrow \infty$ of an infinite domain Ω , Eqs. (30) and (32) lead to Eq. (18), whereas the inverse Laplace transform of the limit of Eqs. (30) and (33) yields Eq. (15).

Small-target limit

For a *small* fixed target in an arbitrary bounded domain Ω' , the asymptotic behavior of the smallest eigenvalue of the Laplace operator has been thoroughly investigated (see [69, 70] and references therein).

For a confining disk of radius \bar{R} , one has [69]

$$\lambda_1 = \frac{2\pi\nu D}{|\Omega'|} - \frac{4\pi^2\nu^2}{|\Omega'|} G(\mathbf{x}_2, \mathbf{x}_2) + O(\nu^3), \quad (42)$$

where $\nu = -1/\ln \varepsilon$, $\varepsilon = \rho/\bar{R}$ is the dimensionless size of the target, $|\Omega'|$ is the area of the shrunk domain Ω' , \mathbf{x}_2 is the location of the target, and $G(\mathbf{x}_2, \mathbf{x}_2)$ is the regular part of the Neumann Green's function:

$$G(\mathbf{x}_2, \mathbf{x}_2) = -\frac{1}{2\pi} F_2(|\mathbf{x}_2|/\bar{R}), \quad (43)$$

where

$$F_2(z) = \frac{3}{4} + \ln(1 - z^2) - z^2, \quad (44)$$

so that

$$\lambda_1 \simeq \frac{2\nu D}{\bar{R}^2} \left(1 + \nu F_2(|\mathbf{x}_2|/\bar{R}) \right). \quad (45)$$

The decay time is then

$$T(\mathbf{x}_2) \simeq \frac{\bar{R}^2 \ln(\bar{R}/\rho)}{2D} \left(1 + \frac{F_2(|\mathbf{x}_2|/\bar{R})}{\ln(\bar{R}/\rho)} \right)^{-1} \quad (\rho \ll \bar{R}). \quad (46)$$

This expression refines Eq. (40), which corresponds to $|\mathbf{x}_2| = 0$, with $F_2(0) = 3/4$. In turn, the above asymptotic relation is not applicable when $|\mathbf{x}_2|$ approaches \bar{R} (i.e., when the target is too close to the boundary) because of the logarithmic divergence of the correction term (see below the asymptotic form of the MFPT, which remains well defined in this limit).

In three dimensions, one has [70]

$$\lambda_1 = D(\varepsilon\lambda^{(1)} + \varepsilon^2\lambda^{(2)} + O(\varepsilon^3)), \quad (47)$$

where

$$\lambda^{(1)} = \frac{4\pi C}{|\Omega'|} = \frac{3}{\bar{R}^3}, \quad (48)$$

and C is the capacitance of the target of unit size (which is equal to 1 in the case of an spherical target). The next-order correction $\lambda^{(2)}$ is again expressed in terms of the regular part of the Neumann Green function. For a spherical confining domain of radius \bar{R} , one has

$$\begin{aligned} \lambda_1 &= \frac{4\pi\rho D}{|\Omega'|} - \frac{16\pi^2\rho^2}{|\Omega'|} G(\mathbf{x}_2, \mathbf{x}_2) + O(\rho^3) \\ &= \frac{3\rho D}{\bar{R}^3} \left(1 - \frac{\rho}{\bar{R}} F_3(|\mathbf{x}_2|/\bar{R}) + O(\rho^2) \right), \end{aligned} \quad (49)$$

where

$$F_3(z) = \frac{1}{1-z^2} - \ln(1-z^2) + z^2 - \frac{14}{5}. \quad (50)$$

As a consequence, the decay time behaves as

$$T(\mathbf{x}_2) \simeq \frac{\bar{R}^3}{3D\rho} \left(1 - \frac{\rho}{\bar{R}} F_3(|\mathbf{x}_2|/\bar{R})\right)^{-1} \quad (\rho \ll \bar{R}). \quad (51)$$

This expression refines Eq. (40), which corresponds to $|\mathbf{x}_2| = 0$, with $F_3(0) = -9/5$, and thus

$$\lambda_1 = \frac{3\rho D}{\bar{R}^3} \left(1 + \frac{9}{5} \frac{\rho}{\bar{R}} + O(\rho^2)\right). \quad (52)$$

Note that this result agrees with the direct asymptotic analysis of the smallest eigenvalue obtained as $\lambda_1 = D\alpha_1^2/\bar{R}^2$, where α_1 is the smallest strictly positive solution of Eq. (38), see [68]. Again, the opposite limit $|\mathbf{x}_2| \rightarrow \bar{R}$ yields the divergent correction term, and thus is not applicable.

The asymptotic behavior of the MFPT to a small target located on the boundary of the domain was given in Ref. [30]:

$$\langle \mathcal{T} \rangle \simeq \frac{|\Omega'|}{2\pi D} \times \begin{cases} \ln(r/\rho) & (d=2), \\ \frac{\Gamma(d/2)}{\pi^{d/2-1}} (\rho^{2-d} - r^{2-d}) & (d \geq 3), \end{cases} \quad (53)$$

where $r = |\mathbf{x}_1 - \mathbf{x}_2|$ is the distance between the target and the starting position of the diffusing particle. For instance, one gets

$$\langle \mathcal{T} \rangle \simeq \frac{\bar{R}^2 \ln(\bar{R}/\rho)}{2D} \left(1 + \frac{\ln(r/\bar{R})}{\ln(\bar{R}/\rho)}\right) \quad (54)$$

for a disk of radius \bar{R} , and

$$\langle \mathcal{T} \rangle \simeq \frac{\bar{R}^3}{3D\rho} \left(1 - \frac{\rho}{r}\right) \quad (55)$$

for a sphere of radius \bar{R} . While the leading terms in both expressions are identical with those in Eqs. (46, 51), the MFPTs depend on the positions of both particles (the searcher and the target), whereas the decay time T depends only on the position of the target.

III. MONTE CARLO SIMULATIONS

In this work, we undertake a systematic study of the FET distribution in two and three-dimensional domains. We restrict our analysis to two particles of identical radii:

$$\rho_1 = \rho_2 = \rho/2. \quad (56)$$

We fix length units by setting $\rho = 1$. In turn, we vary other parameters such as diffusion coefficients (D_1, D_2), the initial positions of particles ($\mathbf{x}_1, \mathbf{x}_2$), and the size of the confinement (R). While both the mathematical

analysis of the boundary value problem (2) – (4) and the associated numerical simulations can be performed for particles of arbitrary size (under the evident geometric constraint $2\rho < R$), we restrict our study to the case of relatively small particles: $\rho \ll R$. Even though the limit of strong confinement (particle diameter comparable to domain diameter) is also interesting for applications, we will focus on systems with relatively small particles.

For a given set of parameters, we simulated individual trajectories of two diffusing particles in confinement and computed their FET \mathcal{T}_i in each run i (see Appendix for technical details). To avoid exceedingly long trajectories, we introduced a cut-off time t_{cut} , at which the simulation was stopped, even if two particles had not met. The cut-off time was large enough to ensure that $S(t_{\text{cut}}|\mathbf{x}_1, \mathbf{x}_2)$ was very small so that the cut-off did not influence the results (see below). The simulation was repeated $N = 10^6$ times to get a good enough FET statistics and to access the long-time behavior of the survival probability. The empirical curves of $S(t|\mathbf{x}_1, \mathbf{x}_2)$ were obtained by dividing the number of realizations with $\mathcal{T}_i > t$ by N , whereas the empirical curves of $H(t|\mathbf{x}_1, \mathbf{x}_2)$ were obtained as renormalized histograms obtained from the values of \mathcal{T}_i .

Even though we will generally display $S(t|\mathbf{x}_1, \mathbf{x}_2)$ and $H(t|\mathbf{x}_1, \mathbf{x}_2)$ for a broad range of timescales, the data corresponding to large times exhibit high statistical uncertainties. In fact, since we use $N = 10^6$ realizations, values of, say, $S(t) \lesssim 10^{-4}$, were estimated with a relatively small number of outcomes and have thus to be taken with care. There exist efficient methods for improving the statistical accuracy of rare events in Monte Carlo simulations. For instance, Nayak *et al.* implemented one such method to access the long-time behavior of the survival probability [63]. As our focus is on the study of the whole distribution of the FET, we keep using the basic Monte Carlo scheme.

The simulation results are systematically compared to the available analytical results and approximations. The survival probability and the FET probability density in the no-boundary case, $S_{\text{free}}(t|\mathbf{x}_1, \mathbf{x}_2)$ and $H_{\text{free}}(t|\mathbf{x}_1, \mathbf{x}_2)$, are given by explicit formulas (15, 17) in the three-dimensional case; in turn, a numerical integration of Eqs. (19, 20) was used in two dimensions. These quantities for the concentric planar case were obtained by a numerical inverse Laplace transform of Eqs. (32, 33), even so spectral expansions can also be obtained via the residue theorem.

The decay time T was estimated from the analysis of the logarithmic derivative of the survival probability. In fact, the long-time relation (13) implies that $-\dot{S}(t)/S(t) \approx 1/T$ over a broad range of times $t \in (t_1, t_2)$. Here t_1 is the timescale above which the long-time relation (13) is applicable, i.e., when the other terms of the spectral expansion (12) can be neglected. Strictly speaking, this timescale is determined by the second eigenvalue of the diffusion operator but in practice, it is sufficient to take t_1 to be of the order of T (e.g., $5T$). The upper limit t_2 , which formally could be infinitely large, is

necessary to eliminate statistical uncertainties in the survival probability due to a limited number of realizations. In practical terms (see Appendix B) we choose the time interval (t_1, t_2) in such a way that, except for statistical uncertainties, $-\dot{S}(t)/S(t)$ remains (approximately) constant. Once the time range (t_1, t_2) is set, the decay time can be estimated as

$$T = \frac{t_2 - t_1}{\int_{t_1}^{t_2} dt (-\dot{S}(t)/S(t))}, \quad (57)$$

while the accuracy of this estimate can be measured by the norm of fluctuations of $-\dot{S}(t)/S(t)$ around $1/T$:

$$\delta T = T^2 \sqrt{\frac{\int_{t_1}^{t_2} dt [-\dot{S}(t)/S(t) - 1/T]^2}{t_2 - t_1}} \quad (58)$$

(see illustrations in Fig. 15 and further discussion in Appendix B).

We emphasize that this estimation procedure is more informative than a direct linear fit of $\ln S(t)$. First, one can choose the appropriate range (t_1, t_2) and also evaluate the error δT . Second, in cases when one particle has a much smaller diffusion coefficient than the other particle, there may exist an intermediate regime, in which the exponential factor $e^{-t/T}$ is affected by a slowly varying prefactor $f(t)$ converging to a constant as $t \rightarrow \infty$. This prefactor may result in a systematic bias in the estimated decay time T . As such a bias is usually small, it is difficult to appreciate from fitting $\ln S(t)$. In turn, its effect becomes more apparent when showing $-\dot{S}(t)/S(t)$.

We also estimated the MFET. As the numerical simulations have been performed with a time cut-off at t_{cut} , one cannot compute directly the MFET by taking an average over realizations \mathcal{T}_i of the first-encounter time. Nevertheless, it can be estimated through other quantities that are directly accessible. The first one is the average of the first-encounter times generated in each run, constrained to be equal to t_{cut} when the particles have not yet met by the time t_{cut} , i.e.

$$\bar{\mathcal{T}} = \frac{1}{N} \sum_{i=1}^N \min\{\mathcal{T}_i, t_{\text{cut}}\}, \quad (59)$$

where \mathcal{T}_i is the first-encounter time in the i -th realization if there were no cut-off. For large N , this empirical average approximates the expectation

$$\begin{aligned} \bar{\mathcal{T}} \xrightarrow{N \rightarrow \infty} \langle \min\{\mathcal{T}, t_{\text{cut}}\} \rangle &= \int_0^{t_{\text{cut}}} dt t H(t) + t_{\text{cut}} \int_{t_{\text{cut}}}^{\infty} dt H(t) \\ &= \int_0^{t_{\text{cut}}} dt S(t) = \langle \mathcal{T} \rangle - \int_{t_{\text{cut}}}^{\infty} dt S(t) \end{aligned} \quad (60)$$

(here we omitted the arguments $\mathbf{x}_1, \mathbf{x}_2$ for brevity). This quantity is clearly a lower bound for the MFET $\langle \mathcal{T} \rangle$.

According to the second line, this estimate corresponds to the truncation of the integral in Eq. (8) at t_{cut} . If $t_{\text{cut}} \gg T$, the long-time behavior of the survival probability can be approximated as

$$S(t) \simeq S(t_{\text{cut}}) \exp(-(t - t_{\text{cut}})/T), \quad (61)$$

so that

$$\langle \min\{\mathcal{T}, t_{\text{cut}}\} \rangle \simeq \langle \mathcal{T} \rangle - T S(t_{\text{cut}}). \quad (62)$$

In this way, one can control the error of the estimate $\bar{\mathcal{T}}$ and choose an appropriate t_{cut} ; in particular, $S(t_{\text{cut}})$ should be very small.

The other manner to estimate the MFET is by computing the average with the conditional probability density:

$$H_{\text{cond}}(t) = H(t) \left(\int_0^{t_{\text{cut}}} dt' H(t') \right)^{-1} \quad (63)$$

(again, the dependence on $\mathbf{x}_1, \mathbf{x}_2$ is omitted here). This density is defined and well normalized for times from 0 to t_{cut} . The corresponding conditional MFET reads then

$$\langle \mathcal{T} \rangle_{\text{cond}} = \int_0^{t_{\text{cut}}} dt t H_{\text{cond}}(t). \quad (64)$$

As t_{cut} goes to infinity, the conditional mean approaches $\langle \mathcal{T} \rangle$. Indeed, one gets

$$\begin{aligned} \langle \mathcal{T} \rangle_{\text{cond}} &= \frac{\langle \mathcal{T} \rangle - t_{\text{cut}} S(t_{\text{cut}}) - \int_{t_{\text{cut}}}^{\infty} dt S(t)}{1 - S(t_{\text{cut}})} \\ &\simeq \frac{\langle \mathcal{T} \rangle - (t_{\text{cut}} + T) S(t_{\text{cut}})}{1 - S(t_{\text{cut}})}, \end{aligned} \quad (65)$$

where we used again the approximation (61) to get the second relation. One sees that $\langle \mathcal{T} \rangle_{\text{cond}}$ is very close to $\langle \mathcal{T} \rangle$ as soon as $t_{\text{cut}} \gg T$. From empirical data, the conditional MFET can be estimated as

$$\bar{\mathcal{T}}^* = \frac{\sum_{i=1}^N \mathcal{T}_i \mathbb{I}_{\mathcal{T}_i \leq t_{\text{cut}}}}{\sum_{i=1}^N \mathbb{I}_{\mathcal{T}_i \leq t_{\text{cut}}}}, \quad (66)$$

where $\mathbb{I}_{\mathcal{T}_i \leq t_{\text{cut}}} = 1$ if $\mathcal{T}_i \leq t_{\text{cut}}$, and 0 otherwise. When $\bar{\mathcal{T}}$ and $\bar{\mathcal{T}}^*$ are close, they are very good estimates of the MFET, as we only neglected some outlier data (in all our simulations $S(t)$ is very small for $t = t_{\text{cut}}$ and decays exponentially for $t > t_{\text{cut}}$, which makes the weight of those outliers negligible).

IV. FIXED TARGET PROBLEM IN 2D

To gain intuition onto the dependence of the FET on the initial positions, we start with the fixed target problem. The comparison of numerical results with available theoretical predictions will serve for validating Monte

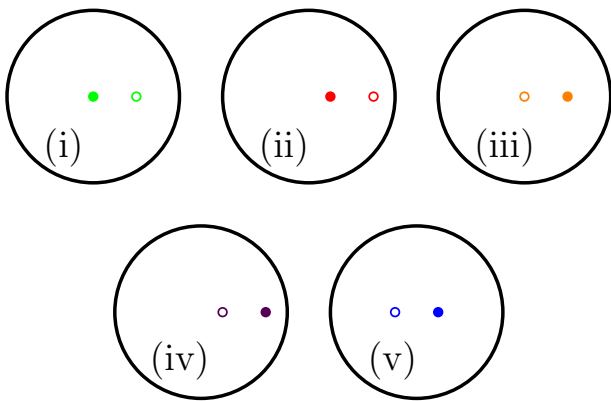


FIG. 1: Five initial configurations with a diffusing particle (empty circle) and a fixed target (filled circle) inside a disk of radius $R = 10$. The initial positions of the centers of the diffusing particle and of the target are: (i) $\mathbf{x}_1 = (5, 0)$ and $\mathbf{x}_2 = (0, 0)$, (ii) $\mathbf{x}_1 = (7.5, 0)$ and $\mathbf{x}_2 = (2.5, 0)$, (iii) $\mathbf{x}_1 = (0, 0)$ and $\mathbf{x}_2 = (5, 0)$, (iv) $\mathbf{x}_1 = (2.5, 0)$ and $\mathbf{x}_2 = (7.5, 0)$, and (v) $\mathbf{x}_1 = (-2.5, 0)$ and $\mathbf{x}_2 = (2.5, 0)$.

Carlo simulations. We consider the confining domain Ω to be a disk of radius $R = 10$ with reflecting boundary; a particle started from \mathbf{x}_1 diffuses with diffusion coefficient $D_1 = 1/2$ towards an immobile target ($D_2 = 0$) fixed at \mathbf{x}_2 . We fix the initial distance between the particles, $|\mathbf{x}_1 - \mathbf{x}_2| = 5$, and consider five configurations shown in Fig. 1.

We will distinguish three regimes: short times ($t \lesssim t_B$) when the boundary does not yet play any role; intermediate times ($t_B \lesssim t \lesssim T$); and long times ($t \gtrsim T$), at which the monoexponential decay of the survival probability is established. Here T is the decay time defined by (29), whereas the time scale t_B will be defined below.

Figure 2(a) presents the survival probabilities for five configurations shown in Fig. 1. At short times, the order in which $S(t)$ first deviates from S_{free} is $S(\text{ii}) \rightarrow S(\text{iv}) \rightarrow S(\text{i}) \rightarrow S(\text{iii}) \rightarrow S(\text{v})$, see Fig. 2(b). The presence of the reflecting boundary implies a reduction of the survival probability with respect to the no boundary case (dashed line). In fact, confinement does not allow the diffusing particle to move too far away from the target. Then, in those initial arrangements where the particles are closer to the boundary, they have more chances to meet earlier. Let us now introduce an empirical time scale t_B to describe when the boundary starts to matter,

$$t_B \equiv \frac{(L_M - \rho/2)^2}{2dD}, \quad (67)$$

where L_M is the distance between the boundary and the middle point of the initial positions of the particles (their centers). With this definition $t_B(\text{ii}) = t_B(\text{iv}) < t_B(\text{i}) = t_B(\text{iii}) < t_B(\text{v})$.

Equation (67) has the drawback that it does not recognize that the time at which the boundary starts to matter, is shorter for case (ii) than for case (iv), and also shorter for case (i) than for case (iii) (see Fig. 2(b)). The

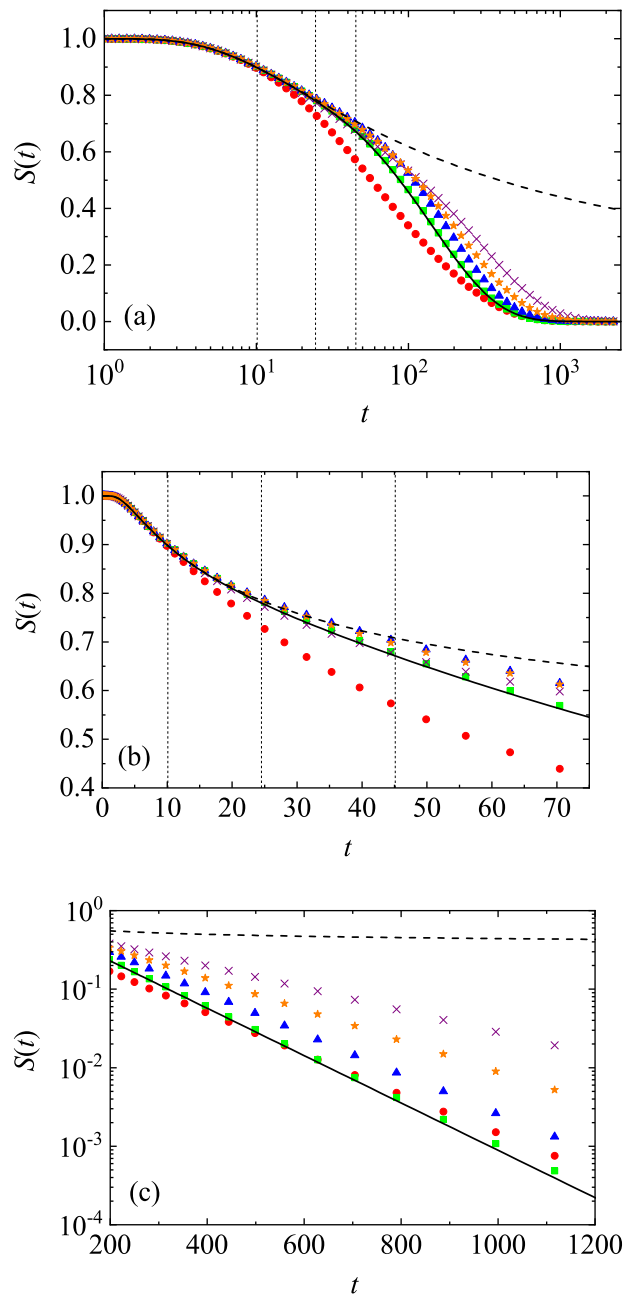


FIG. 2: Survival probability versus time for a particle of diffusion coefficient $D_1 = 1/2$ in the search for a fixed target inside a disk of radius $R = 10$. Symbols present $S(t|\mathbf{x}_1, \mathbf{x}_2)$ for five configurations of \mathbf{x}_1 and \mathbf{x}_2 described in Fig. 1: squares (i), circles (ii), stars (iii), crosses (iv), and triangles (v). Solid line is the exact solution for case (i), obtained by numerical Laplace inversion of Eqs. (30) and (32). Dashed line shows $S_{\text{free}}(t|\mathbf{x}_1, \mathbf{x}_2)$ from Eq. (19). Vertical dashed lines indicate the values of t_B : 10.1 for cases (ii) and (iv), 24.5 for cases (i) and (iii), and 45.1 for case (v). Note that t_B corresponds to the time at which $S(t)$ separates from $S_{\text{free}}(t)$ for cases (i), (ii) and (v), but not for cases (iii) and (iv). Panels (a, b, c) illustrate different aspects of the same survival probabilities.

reason for this behavior is that for cases (ii) and (i) the diffusing particle starts from the position that is closer to the boundary and it is therefore likely for the diffusing particle to find the boundary rapidly and then to move towards the target along the boundary [71]. In turn, if the target is closer to the boundary, the particle can get farther both from the target and the boundary at short times.

The latter argument can be extended to explain the long-time behavior of the survival probability. For some locations of the target, there could be extended regions in which the moving particle may diffuse for a long time without approaching the target. In particular, when the target is centered, the survival probability at long times is expected to be the smallest one, as confirmed by simulations. In this particular case, the sum of the distances from the starting point of the moving particle to the target and to the boundary is constant, i.e., it does not depend on the starting position of the moving particle.

Figure 2(c) illustrates the exponential decay (28) of the survival probability at long times, with the decay time $T(\mathbf{x}_2)$ given by Eq. (29). Table I provides T for the initial configurations (i)-(v) described above. The values of T differ from each other, except for the cases (ii) and (v), where $T \simeq 165$, highlighting the dependence of T on the position of the target but not on the initial position on the diffusing particle. Expectedly, the smallest T is observed for the centered target, while the configurations (iii) and (iv) yield larger T as the target is located far from the center of the disk (note that a similar effect for the MFET $\langle \mathcal{T} \rangle$ was reported in [12]). The values of T estimated from Monte Carlo simulations are in excellent agreement with their theoretical predictions from Eq. (29). We also stress that the decay time T is in very good agreement with its approximation by the small-target asymptotic formula (46), except for the case (iv), in which the target is too close to the boundary, and Eq. (46) is not applicable. We emphasize that the second-order term in Eq. (46) is significant: the leading-order approximation (such as Eq. (40)) would give $T \approx 203$ for all initial configurations.

In Table I we also provide the values of two estimates $\bar{\mathcal{T}}$ and $\bar{\mathcal{T}}^*$ of the MFET. For the case (i), Eq. (34) yields the MFET $\langle \mathcal{T} \rangle \approx 133$, which differs by only 2% from both estimates $\bar{\mathcal{T}}$ and $\bar{\mathcal{T}}^*$. When comparing the cases (ii) and (v), one observes that their MFETs are quite distinct, as opposed to almost identical values of T in these cases. The initial configuration (ii) leads to a lower MFET than (v) because the center of mass is closer to the boundary, favoring the encounter of two particles at shorter times. This example illustrates the dependence of the MFET on the initial position. Besides, the estimates of the MFET are close to T in the cases (i) and (v). In the case (v), the target is close to the center of the disk (that avoids large void regions), and the relevance of the boundary appears at larger times than in the other cases. Notice that, roughly, the following rule-of-thumb holds: the sooner $S(t)$ separates from S_{free} , the better

Case	Decay time			MFET		
	T_{num}	T_{asympt}	$T_{\text{simu}}(\delta T)$	$\bar{\mathcal{T}}_{\text{num}}$	$\bar{\mathcal{T}}$	$\bar{\mathcal{T}}^*$
(i)	144	152	146 (3.6)	133	136	136
(ii)	165	174	167 (4.5)	108	110	110
(iii)	218	231	219 (3.6)	184	187	187
(iv)	305	558	308 (4.0)	228	231	230
(v)	165	174	167 (5.1)	157	160	160

TABLE I: Several estimates of the decay time T and MFET $\langle \mathcal{T} \rangle$ for the cases of Fig. 1. Here $T_{\text{num}} = 1/\lambda_1$ is obtained by means of the numerical computation of the first eigenvalue λ_1 of the Laplace operator by a finite-element method (implemented in the PDEtool, Matlab). The result for case (i) agrees with the exact value provided by Eq. (37). T_{asympt} is obtained by the small-target asymptotic formula (46), T_{simu} is the value estimated from Monte Carlo simulations and δT are the corresponding errors obtained from Eq. (58). Note that the value of T_{asympt} for (iv) is too large because the target is located near the boundary, and so Eq. (46) is not applicable. On the other hand, $\bar{\mathcal{T}}_{\text{num}}$ is the estimate of $\langle \mathcal{T} \rangle$ obtained by solving numerically the boundary value problem Eqs.(9)-(11) by a finite-element method (FEM) implemented in PDEtool, Matlab. Finally the two estimates $\bar{\mathcal{T}}$ and $\bar{\mathcal{T}}^*$ of the MFET from Eqs. (59) and (66) are also given. A minor but systematic difference between $\bar{\mathcal{T}}_{\text{num}}$ and these two estimates can potentially be attributed to discretization effects in both numerical methods (spatial discretization of FEM and temporal discretization in Monte Carlo simulations).

the agreement between the MFET and T is. This will also be seen to be case for two diffusing particles (see Sec. VB and VI).

In summary, the survival probability in confinement changes, especially at long times, if the initial positions of a diffusing particle and a fixed target are swapped, unless the problem preserves the symmetry after the swap (e.g. in the case (v)).

Figure 3 illustrates the FET probability density $H(t|\mathbf{x}_1, \mathbf{x}_2)$. Let first note that the simulations for the case (i) manifest an excellent agreement with theory. One observes that the densities coincide with the solution $H_{\text{free}}(t|\mathbf{x}_1, \mathbf{x}_2)$ for the no boundary case at least until t_B . At long times, the densities exhibit an exponential decay, with the decay time T depending the position of the target, as expected.

V. IDENTICAL DIFFUSING PARTICLES

In this section, we will see what happens if the fixed target starts to diffuse as the other particle. In other words, we study the statistics of the first-encounter time for two identical diffusing particles with $D_1 = D_2 = D/2$, confined in a disk of radius R with reflecting boundary.

In the no boundary case, there is no difference between the problem with a fixed target and the problem with two diffusing particles, as the survival probability, given by Eq. (19), depends on the sum of diffusion coefficients.

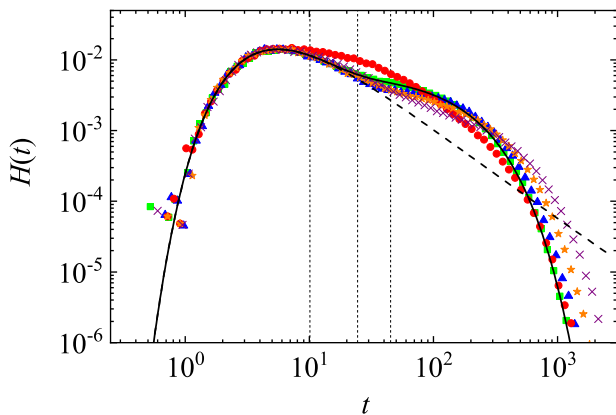


FIG. 3: FET probability density versus time for a particle of diffusion constant $D_1 = 1/2$ in the search for a fixed target inside a disk of radius $R = 10$. Symbols present simulation results for five configurations shown in Fig. 1: squares (i), circles (ii), stars (iii), crosses (iv), and triangles (v). Solid line shows the exact solution for the case (i), obtained by numerical Laplace inversion of Eq. (32). Dashed line is $H_{\text{free}}(t|\mathbf{x}_1, \mathbf{x}_2)$ from Eq. (20). Vertical dashed lines indicate the values of t_B : 10.1 for cases (ii) and (iv), 24.5 for cases (i) and (iii), and 45.1 for case (v).

However, in the presence of a reflecting boundary, these two problems are no longer equivalent and we will compare them in this section.

A. Two timescales

First, we identify two timescales that control the behavior of the survival probability: t_F , at which two particles *typically* meet for the first time in the no boundary case, and t_B , above which the influence of the boundary cannot be neglected. The timescale t_F can be defined as the most probable FET, i.e., the time at which the FET density $H_{\text{free}}(t|\mathbf{x}_1, \mathbf{x}_2)$ is maximal [64]. In three dimensions, taking the time derivative of the explicit formula (15) and equating it to 0 yield

$$t_F = \frac{(r - \rho)^2}{6D}. \quad (68)$$

In two dimensions, it was argued that Eq. (68) still gives an accurate estimate of the most probable FET [36]. We emphasize that the factor 6 in the denominator does not depend on the space dimensionality, given that the short-time asymptotic behavior of the PDF is given by $e^{-(r-\rho)^2/(4Dt)}/t^{3/2}$ in all dimensions.

The second timescale t_B might naively be thought as being determined by the initial distance from each particle to the boundary. Such a distance would indeed determine a timescale for interaction of a single particle to the boundary. However, as we are interested in the first-encounter time between two particles, the initial distances between the particles and the boundary are less

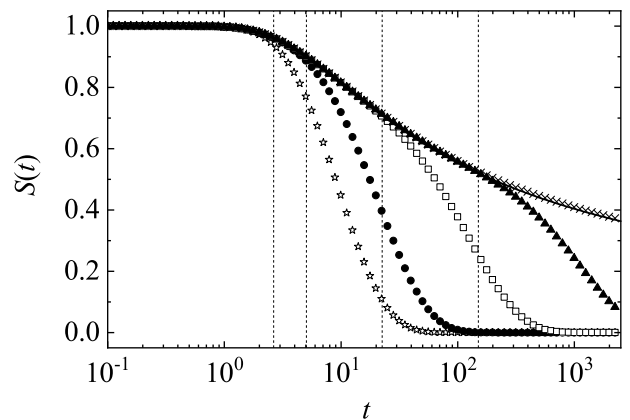


FIG. 4: Survival probability versus time for two diffusing particles with equal diffusion coefficients $D_1 = D_2 = 1/2$ that are initially placed at $(-2.5, 0)$ and $(0, 2.5)$ inside a disk of radius R . Symbols present simulation results for $R = 3.75$ (stars), $R = 5$ (circles), $R = 10$ (squares), $R = 25$ (triangles), and no boundary (crosses). Solid line shows $S_{\text{free}}(t|\mathbf{x}_1, \mathbf{x}_2)$ from Eq. (19). Vertical dashed lines indicate the values of t_B : 2.6, 5.1, 22.6, and 150. Here $t_F \simeq 2.7$.

relevant. In contrast, if the particles are diametrically opposed and very close to the boundary, the boundary starts to affect the motion of each particle at very early times, but these times are not so relevant for the first-encounter time, at least for small particles. For this reason, we keep using t_B defined by Eq. (67), as justified below.

Now we can study how the survival probability depends on the size of the domain and on the initial positions of the particles. We first plot in Fig. 4 the survival probability for two particles initially placed at $\mathbf{x}_1 = (-2.5, 0)$ and $\mathbf{x}_2 = (0, 2.5)$ for different values of the domain radius R . As expected, all simulation results coincide with $S_{\text{free}}(t|\mathbf{x}_1, \mathbf{x}_2)$ until $\sim t_B$ corresponding to each value of R . It is also observed that the survival probability decays faster for lower R .

Next, Fig. 5(a) shows the survival probability for three initial configurations with fixed $R = 10$. In configurations (i) and (ii), the center of mass of the two particles is at the origin, implying the same time $t_B \simeq 22.6$ according to Eq. (67). One observes that the deviation from the no boundary case occurs around this time, even though the two particles are much closer to the boundary in the case (ii). The survival probability at t_B is smaller in the case (i). In turn, in configurations (i) and (iii), the initial distances between the centers of the particles is the same, but both particles are shifted towards the boundary in the case (iii). The corresponding survival probabilities are different, highlighting their dependence on the initial positions of both particles (not only on their initial distance, as in the no boundary case). In particular, the simulation results deviate from $S_{\text{free}}(t|\mathbf{x}_1, \mathbf{x}_2)$ with $r = 5$ around $t_B \simeq 5.1$. We conclude that the center of mass is a useful indicator of the time scale t_B at

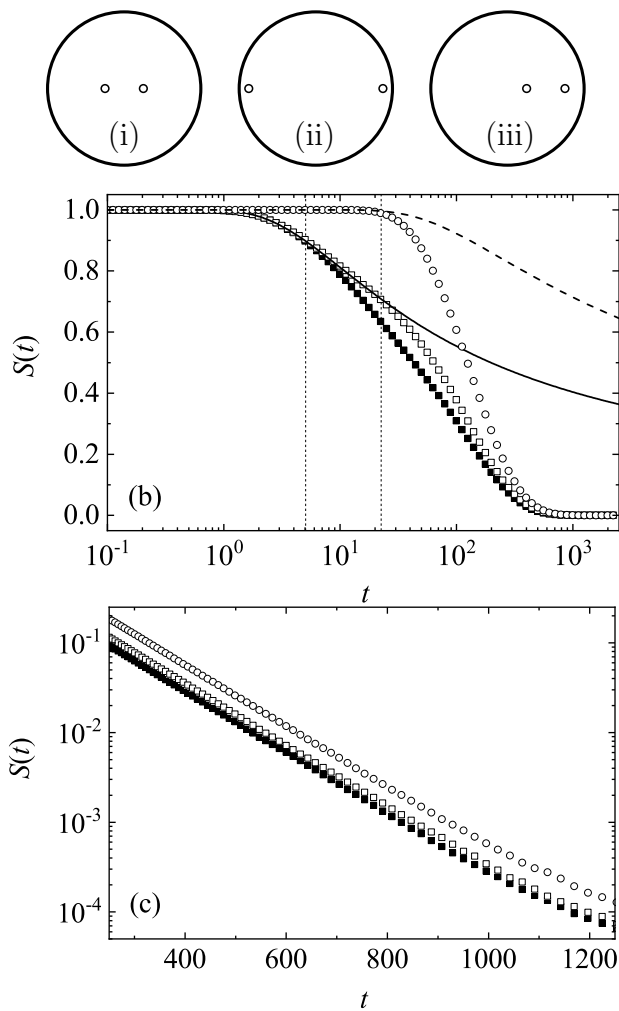


FIG. 5: (a) Three initial configuration of two diffusing particles with equal diffusion coefficients $D_1 = D_2 = 1/2$ inside a disk of radius $R = 10$, with the initial positions: (i) $(-2.5, 0)$ and $(2.5, 0)$, (ii) $(-8.75, 0)$ and $(8.75, 0)$, and (iii) $(0, 2.5)$ and $(0, 7.5)$. (b) Survival probability versus time over a broad range of times (logarithmic scale for horizontal axis); (c) Long-time behavior (logarithmic scale for vertical axis). Symbols refer to the above configurations: (i) empty squares, (ii) circles, and (iii) filled squared. Lines represent $S_{\text{free}}(t|\mathbf{x}_1, \mathbf{x}_2)$ from Eq. (19) for the initial inter-particle distances $r = 5$ (solid) and $r = 17.5$ (dashed). Vertical dashed lines indicate the values of $t_B = 5.1$ [case (iii)] and $t_B = 22.6$ [cases (i) and (ii)].

which the survival probability starts to differ from its counterpart in the no boundary case.

B. Long-time decay

While the above discussion focused on the short-time behavior, we now study the survival probability at long times: $t \gg \max\{t_B, t_F\}$. As the confining domain Ω is bounded, the survival probability exhibits an expo-

ponential decay (13). We estimate the decay time T from Fig. 5(b) and analyze the dependence of T on the parameters. For three initial configurations, the numerical points follow parallel straight lines, while their linear fit yields the same decay time $T = 127 \pm 5$ (see Table II). In fact, the initial condition appears only in the prefactor in Eq. (13), which shifts the curves vertically. In other words, at long times, the system almost forgets about the initial condition, in contrast to the case of a fixed target, where T varied with the position of the target.

In the small target limit, $\rho \ll \bar{R}$, it is instructive to check whether the asymptotic formula (40), derived in the case of a fixed target, is valid for two diffusing particles with $D = D_1 + D_2 = 2D_1$:

$$T \simeq \frac{\bar{R}^2}{2D} \ln(\bar{R}/\rho) \quad (\rho \ll \bar{R}). \quad (69)$$

A similar claim for the MFET was recently proved in the three-dimensional case [62]. First, we observe in Fig. 6 that T is indeed proportional to $1/D$. Each point corresponds to a different value of the diffusion coefficient $D = 2D_1$. A linear fit in the double logarithmic scale yields the expected slope of -1 . Second, we analyze in Fig. 7 how T changes with the size \bar{R} of the confining domain. We find that our simulation results are well described by the formula

$$T \simeq \frac{\bar{R}^2}{2D} \left(C_2 \ln(\bar{R}/\rho) + A(D_1/D_2) + \dots \right), \quad (70)$$

where $C_2 = 1$, $A(D_1/D_2)$ is a dimensionless function of D_1/D_2 , and \dots refers to next-order corrections, which are small for $\rho \ll \bar{R}$ and not accessible from our simulations. Even though this section was focused on identical particles with $D_1 = D_2$, i.e., only one value $A(1)$, we keep the general form $A(D_1/D_2)$ that will be discussed for $D_1/D_2 \neq 1$ in Sec. VI. This means that the asymptotic formula (40) for a fixed target reproduces the main logarithmic term for the case of two diffusing particles. Expectedly, the leading term in Eq. (70) with $D = 2D_1$ is twice smaller than that in Eq. (40) with $D = D_1$, i.e., the decay is faster in the present case of two identical searchers. In other words, to obtain the same asymptotic decay for a fixed target, the searcher would need to have the twice larger diffusivity. We also outline that the leading (logarithmic) term in Eq. (70) is inaccurate due to the existence of the $O(1)$ correction term $A(D_1/D_2)$, as confirmed by our simulations. Getting a rigorous derivation of Eq. (70) and finding the correction term $A(D_1/D_2)$ present an interesting open problem. Note that other properties of the decay time, such as its dependence on the number of searchers, were investigated in [63].

C. MFET

Another important quantity is the MFET defined in Eq. (8). Table II provides the values of two estimates

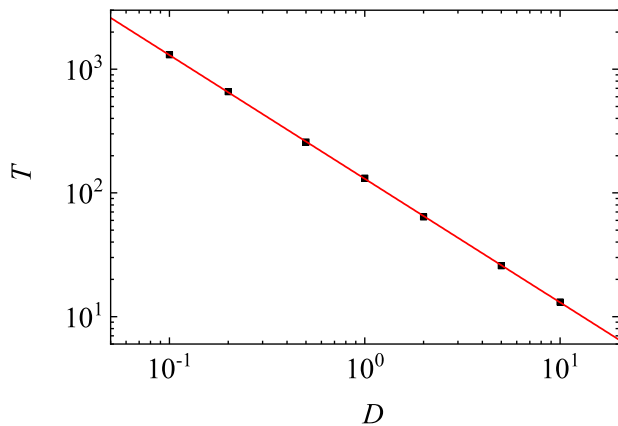


FIG. 6: The decay time T versus D for two diffusing particles with $D_1 = D_2 = D/2$ placed initially at $(0, 0)$ and $(2.5, 0)$ in a disk of radius $R = 10$. Squares represent simulation results, while solid line is a linear fit with slope -1 .

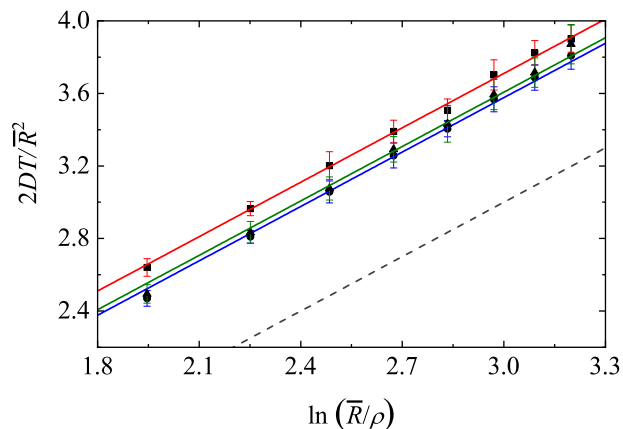


FIG. 7: Scaled decay time $2DT/\bar{R}^2$ versus $\ln(\bar{R}/\rho)$ for two diffusing particles inside a disk of radius R , ranging from 7.5 to 25. Symbols show the simulation results for $D_1 = 0.9$ and $D_2 = 0.1$ (squares), $D_1 = D_2 = 0.5$ (circles), and $D_1 = 1$ and $D_2 = 0.5$ (triangles). Particle 2 (the one with the smallest diffusion coefficient) is initially placed at the center whereas particle 1 is placed at $(5, 0)$. The solid lines correspond to Eq. (70) with $C_2 = 1$ and, from top to bottom, $A(0.9/0.1) = 0.71$, $A(1/0.5) = 0.61$, and $A(0.5/0.5) = 0.58$, respectively. As a reference, the dashed line represents the case with no correction term ($A = 0$).

\bar{T} and \bar{T}^* of the MFET for the three initial configurations shown in Fig. 5(a). In contrast to the decay time T , the MFET depends on the initial positions of the particles. Interestingly, the MFET can be either smaller, or larger than T (recall that in the case of a fixed target, we always observed that the MFET is smaller than T , cf. Table I). In the small target limit, the main contribution to the MFET comes from long trajectories that explore the whole confining domain and correspond to the exponential decay of the survival probability. In this limit, the MFET is typically of the order of T , while its variations can be caused by the prefactor in Eq. (13)

Case	Decay time		MFET	
	T (δT)	\bar{T}	\bar{T}^*	
(i)	126 (2.4)	107	107	
(ii)	127 (2.9)	162	162	
(iii)	127 (4.9)	91	91	

TABLE II: The decay time T , estimated error δT , and two estimates \bar{T} and \bar{T}^* of the MFET from Eqs. (59, 66), for two diffusing particles with $D_1 = D_2 = 1/2$ inside a disk of radius $R = 10$. The initial positions of the particles are: (i) $\mathbf{x}_1 = (-2.5, 0)$ and $\mathbf{x}_2 = (2.5, 0)$; (ii) $\mathbf{x}_1 = (-8.75, 0)$ and $\mathbf{x}_2 = (8.75, 0)$; (iii) $\mathbf{x}_1 = (2.5, 0)$ and $\mathbf{x}_2 = (7.5, 0)$, see Fig. 5. Note that Eq. (69) underestimates the decay time as $T \approx 101.6$, whereas the inclusion of the correction term $A(1) \approx 0.58$ in Eq. (70) gives $T \approx 127.8$, in perfect agreement with the Monte Carlo estimate.

which depends on the initial positions of both particles. One can observe a clear correlation between this prefactor (that shifts the curves in Fig. 5 (b)) and the values of the MFET in Table II.

D. Probability density

To further highlight the relevance of the boundary, we study the shape of the FET probability density $H(t|\mathbf{x}_1, \mathbf{x}_2)$. In the no boundary case, this density has a single hump around t_F : as t grows, the probability of first encounter initially increases (as both particles need to travel a minimum distance to meet), and then slowly decreases (as particles can diffuse too far away from each other). The extremely slow decay (21) of $H_{\text{free}}(t|\mathbf{x}_1, \mathbf{x}_2)$ leads to infinite MFET.

The reflecting boundary changes completely this long-time behavior, given that $H(t|\mathbf{x}_1, \mathbf{x}_2)$ exhibits an exponential decay inherited from Eq. (13). In fact, the boundary prevents diffusing particles from moving far away from each other, thereby eliminating too long trajectories that were possible in the no boundary case.

In Fig. 8 we show the FET probability density for two particles, whose centers were initially placed at $(-2.5, 0)$ and $(2.5, 0)$, with several values of the boundary radius $R = 3.75, 5, 10, \text{ and } 25$. Hence, in these cases, $t_B = 2.6, 5.1, 22.6, \text{ and } 150$, respectively, but $t_F = 2.7$ is the same. As t_B increases, the FET probability density coincides with $H_{\text{free}}(t|\mathbf{x}_1, \mathbf{x}_2)$ over a broader range of times $t < t_B$ and thus widens. When $t_B \gg t_F$, one observes the emergence of a second hump around t_B .

Similar arguments can be used to describe Fig. 9 that shows the FET probability density for three different configurations of particles in the same bounded domain with $R = 10$ (as illustrated in Fig. 5(a)). In cases (i) and (iii), the inter-particle distance $r = 5$ is the same, and two probability densities are close to each other (with the maximum around the same $t_F \simeq 2.7$), even so they start deviating from $H_{\text{free}}(t|\mathbf{x}_1, \mathbf{x}_2)$ at different times t_B . In turn, the case (ii) with a larger distance $r = 17.5$ has

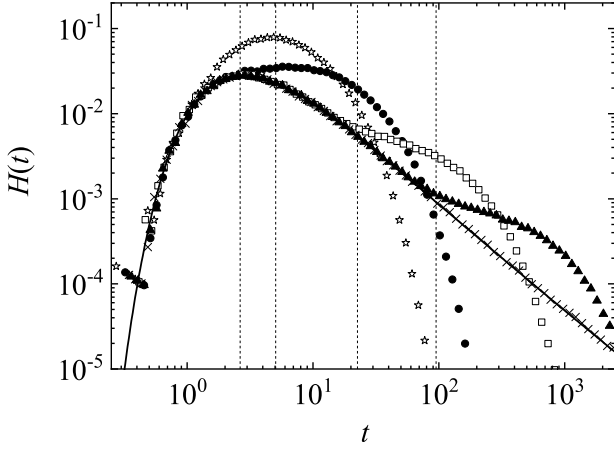


FIG. 8: FET probability density versus time for two diffusing particles of diffusion constants $D_1 = D_2 = 1/2$, initially placed at $(-2.5, 0)$ and $(0, 2.5)$ inside a disk of radius R . Symbols represent simulation results for $R = 3.75$ (stars), $R = 5$ (circles), $R = 10$ (squares), $R = 25$ (triangles), and $R = \infty$ (crosses). Solid line shows $H_{\text{free}}(t|\mathbf{x}_1, \mathbf{x}_2)$ from Eq. (20). Vertical dashed lines indicate the values of t_B : 2.6, 5.1, 22.6, and 150.

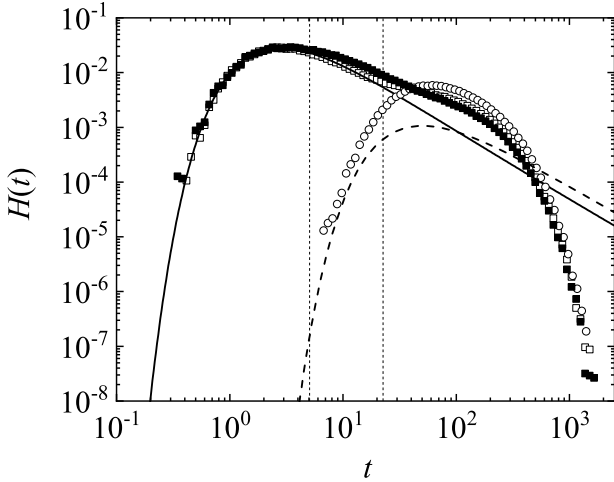


FIG. 9: FET probability density versus time for two diffusing particles of diffusion constants $D_1 = D_2 = 1/2$ inside a disk of radius $R = 10$, with the initial positions of the particles: (i) $(-2.5, 0)$ and $(2.5, 0)$ (empty squares), (ii) $(-8.75, 0)$ and $(8.75, 0)$ (circles), and (iii) $(0, 2.5)$ and $(0, 7.5)$ (filled squares), see Fig. 5. Lines represent $H_{\text{free}}(t|\mathbf{x}_1, \mathbf{x}_2)$ from Eq. (20) with the initial inter-particle distances $r = 5$ (solid) and $r = 17.5$ (dashed). Vertical dashed lines indicate the values of $t_B = 5.1$ [case (iii)] and $t_B = 22.6$ [cases (i) and (ii)].

larger $t_F \simeq 45.4$ so that the maximum of the FET probability density is shifted toward longer times. As $t_B \simeq 22.6$ here is smaller than t_F , the FET density exhibits considerable deviations from $H_{\text{free}}(t|\mathbf{x}_1, \mathbf{x}_2)$ over the relevant range of times. Finally, all the densities are very close to each other at long times, given that the decay time T does not depend on the initial positions of the particles.

VI. TRANSITION FROM IMMOBILE TO MOBILE TARGET

In Sec. IV and Sec. V, we studied separately two scenarios of bimolecular reactions: a diffusing particle searching for a fixed target, and two identical diffusing particles searching to meet one another. These scenarios exhibited different properties because the fixed target introduced a memory on the initial condition that affects the behavior of the survival probability both at short and long times. Here, we consider particles with different diffusion coefficients to study transition between two scenarios. In fact, as the diffusion coefficient D_2 stands in front of the Laplace operator in Eq. (2), the limit $D_2 \rightarrow 0$, corresponding to a fixed target scenario, is singular. This is the mathematical origin of distinct behaviors of the survival probability in the above two scenarios. In physical terms, the timescale associated with the motion of the second particle, L^2/D_2 , is infinite at $D_2 = 0$ (here L is an appropriate length scale, e.g., $L = R$). In turn, if D_2 is small (as compared to D_1) but strictly positive, one can expect that the survival probability behaves at times $t \ll L^2/D_2$ as in the case of a fixed target, and then switches to the behavior for two mobile particles at longer times $t \gtrsim L^2/D_2$. In other words, a smooth transition between two scenarios can be expected.

To clarify this transition, we run simulations for particles with different D_1 and D_2 such that $D = D_1 + D_2 = 1$ is fixed. The first particle is located at the center of a disk of radius $R = 10$ and the second one is at a distance $r = 2.5$. The survival probability is shown in Fig. 10(a) for five cases: (i) $D_1 = 0, D_2 = 1$, (ii) $D_1 = 0.1, D_2 = 0.9$, (iii) $D_1 = D_2 = 0.5$, (iv) $D_1 = 0.9, D_2 = 0.1$, and (v) $D_1 = 1, D_2 = 0$. In this setting, $t_B \simeq 22.6$ for all cases so that the survival probabilities remain close to $S_{\text{free}}(t|\mathbf{x}_1, \mathbf{x}_2)$ for $t \lesssim t_B$. Afterwards, the curves start to deviate from each other, showing that the survival probability depends explicitly on D_1 and D_2 , and not only on their sum.

The long-time behavior of the survival probability is detailed in Fig. 10(b). If one of the particles is fixed (cases (i) and (v)), the survival probability exhibits a faster decay as compared to the cases (ii)-(iv) when both particles diffuse. One sees that when the sum of the diffusion coefficients is fixed, setting one of them equal to zero seems to be detrimental to the survival probability at long times. This statement can be called the “anti-Pascal principle”, by opposition to the “Pascal principle”. The latter states that the survival probability of a mobile target is less than or equal to the survival probability of an immobile target when the diffusion coefficient of the moving particle is fixed [46]. In other words, if the diffusion coefficient of a “hunter” is fixed, an immobile “prey” has more chances to survive than a mobile one. However, when the sum of diffusion coefficients is fixed, the motion of the “hunter” is slower if the “prey” also diffuses, and thus the mobile “prey” survives longer. The fastest decay corresponds to the case (i) when the fixed

			Decay time		MFET	
	D_1	D_2	T (δT)	\bar{T}	\bar{T}^*	
(i)	0	1	75 (3.1)	69	69	
(ii)	0.1	0.9	133 (2.3)	90	90	
(iii)	0.5	0.5	127 (3.3)	103	103	
(iv)	0.9	0.1	134 (4.0)	107	107	
(v)	1	0	110 (3.5)	94	94	

TABLE III: The decay time T and two estimates \bar{T} and \bar{T}^* of the MFET from Eqs. (59, 66), for two diffusing particles inside a disk of radius $R = 10$. The particle with diffusion coefficient D_1 is initially located at $(0, 0)$, whilst the particle with diffusion coefficient D_2 is initially at $(5, 0)$. For cases (i) and (v), the small-target asymptotic formula (46) yields $T \approx 76.2$ and $T \approx 115.7$, in excellent agreement with simulation results. The exact value of T for case (i) is 72.0 whereas $\langle T \rangle$ is 66.6. Note that the estimated value of T here is twice smaller than that from the case (i) in Table I because the diffusion coefficient D_1 was twice smaller in that case. For case (v), the numerical solution of the corresponding boundary value problem leads to $T \simeq 108.8$ and $\langle T \rangle \simeq 92.2$.

target is located at the center of the disk because it is the most accessible for the diffusing particle, implying faster encounters.

While the decay time is clearly different for cases (i) and (v) with a fixed target, the long-time behavior of the survival probability in cases (ii)-(iv) is rather similar. In fact, according to Eq. (13), the decay rate T is independent of the starting positions, i.e., it should be the same for cases (ii) and (iv). This is confirmed by our simulations (see also the estimated values in Table III). In turn, the decay time in the case (iii) of equal diffusivities is by 4% smaller than in cases (ii) and (iv). We note, however, that such a small difference could still be an artifact of numerical simulations or of an estimation procedure from the datapoints, for which the monoexponential decay may not be fully established at the available time scales.

Another important point is the prefactor, which is responsible of the weak dependence of the long-time exponential decay of the survival probability on the initial condition, as in the case of identical particles. This prefactor can lead to different MFETs, depending on whether the particle is close to the boundary or not. Two estimates of the MFET are provided in Table III. One observes that encounters are faster when the particle with the larger diffusion coefficient is close to the boundary.

Similarly, the FET probability densities are also close to each other (Fig. 10(c)). In all considered cases, the probability densities exhibit a single maximum around $t_F \simeq 4$. Interestingly, at times $t \gtrsim t_B$, the presence of the reflecting boundary shifts the probability densities upwards, as compared to the free case (dashed line). A visual inspection suggests the possible presence of inflection point(s) for the curve $H(t|\mathbf{x}_1, \mathbf{x}_2)$.

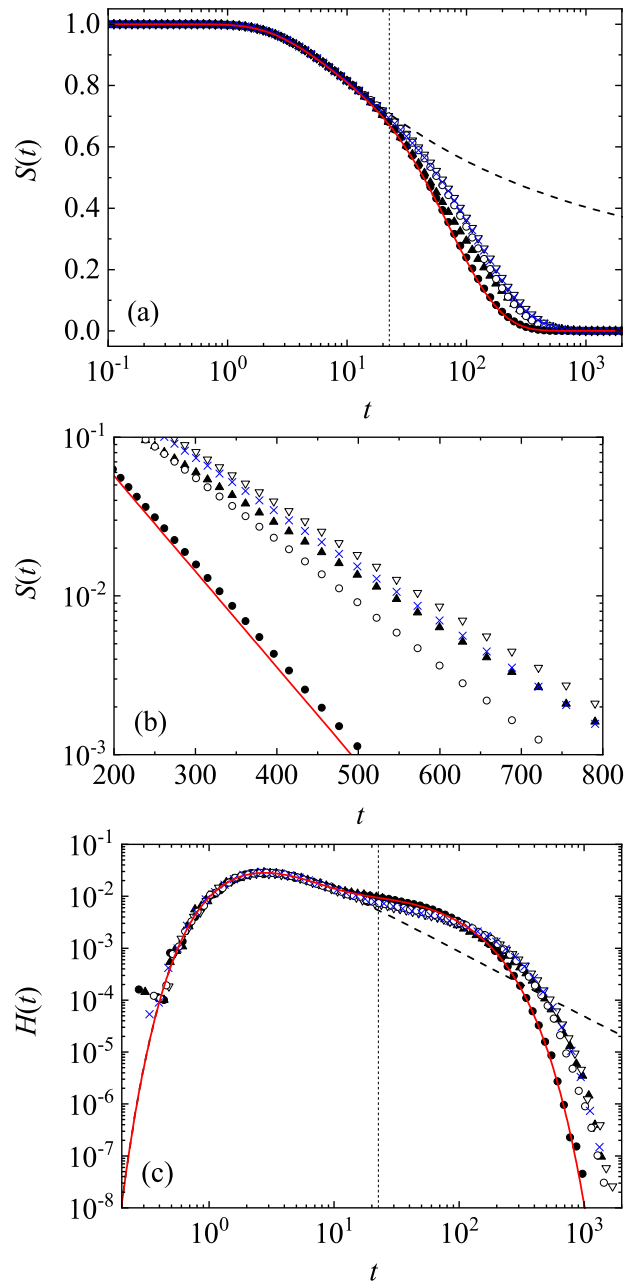


FIG. 10: (a,b) Survival probability for two diffusing particles with: (i) $\{D_1, D_2\} = \{0, 1\}$ (filled circles), (ii) $\{1/10, 9/10\}$ (filled triangles), (iii) $\{1/2, 1/2\}$ (crosses), (iv) $\{9/10, 1/10\}$ (empty triangles), and (v) $\{1, 0\}$ (empty circles). In the initial state, the particle with diffusion constant D_1 is located at $(0, 0)$ and the other is placed at $(5, 0)$ inside a disk of radius $R = 10$. Solid line is the exact solution for the case $\{D_1, D_2\} = \{0, 1\}$ and dashed line presents $S_{\text{free}}(t|\mathbf{x}_1, \mathbf{x}_2)$. Vertical dashed line indicates the value of $t_B = 22.6$. (c) FET probability density for the same configurations. Short-time deviations are caused by the binning artifact and a limited number of realizations with small FET.

The limit of very slow targets

It is instructive to examine in detail the slow-target limit $D_1/D_2 \rightarrow 0$ when the sum of diffusion coefficients is fixed. Figure 11 illustrates the behavior of the survival probability for several values of D_1 : 0, 0.01, 0.02, 0.05, 0.1, 0.25 and 0.5, with $D_2 = 1 - D_1$. For short times ($t \lesssim t_B$), all the lines of $S(t)$ go along the static target line ($D_1 = 0$) and, after a certain time, begin to separate from it. The smaller D_1 is, the larger this time becomes. In this intermediate time range, $S(t)$ cannot be described as $\propto \exp(-t/T)$, since it includes a slowly varying prefactor. After a while, the lines separate from the target line and bend towards the line $D_1 = D_2 = 0.5$, which is reached (within the resolution of the figure or simulation errors, that is, within a given relative error) after a certain time t_J . What we see is that the smaller D_1 is, the larger t_J gets. These moments are marked with short colored arrows. After these times t_J , the lines run together, so that their slope is the same, which means that T is the same, as it should be.

Since the diffusion operator $D_1 \Delta_{\mathbf{x}_1} + D_2 \Delta_{\mathbf{x}_2}$ depends on both D_1 and D_2 , its eigenvalues and thus the decay time $T(D_1, D_2)$ is *a priori* a function of both diffusion coefficients D_1 and D_2 . Even if their sum is fixed, the decay time is still expected to depend on the ratio D_1/D_2 . However, our numerical results and above arguments suggest that, even for not too large confining volumes, $T(D_1, D_2)$ is, to a very good approximation, a function of $D_1 + D_2$ alone (if $D_1 > 0$ and $D_2 > 0$); in this sense, the behavior is reminiscent of the no boundary case. This is an important and counter-intuitive result, which differs from the one-dimensional setting [64], in which the decay time was indeed a function of both D_1 and D_2 . In turn, the characteristic time t_J for relaxation into the monoexponential regime depends on D_1 . In the limit $D_1 \rightarrow 0$, t_J seems to diverge, indicating the singular character of this limit. In other words, as $D_1 \rightarrow 0$, $T(D_1, D_2)$ does not necessarily converge to $T(0, D_2)$ for the static target. The singular character of this limit was established in [64] for one-dimensional diffusion on an interval. In higher dimensions, it would appear that the above arguments still carry over, and we therefore conjecture that the singular behavior would also hold. However, a more rigorous analysis is required. Note, for instance, that the estimates of the decay time in Table III for the cases with finite diffusivities differ, although by 5% only. Concomitantly, we also observe a very weak dependence of the coefficient $A(D_1/D_2)$ on the ratio D_1/D_2 (cf. Fig. 6).

VII. RESULTS IN THREE DIMENSIONS

Finally, we briefly extend our study to the three-dimensional case when two spherical particles of equal radii $\rho_1 = \rho_2 = \rho/2 = 1/2$ diffuse with diffusion coefficients D_1 and D_2 inside a sphere of radius R with

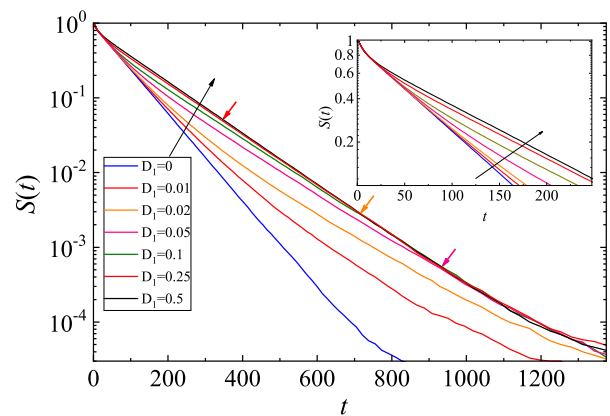


FIG. 11: Survival probability $S(t)$ vs time t for different values of D_1 : 0, 0.01, 0.02, 0.05, 0.1, 0.25 and 0.5, with $D_2 = 1 - D_1$. The first particle starts from the center and the second particle from $(5, 0)$ with $R = 10$. The inset displays the short-time behavior. Arrows indicate the time t_J discussed in the text.

reflecting boundary. The results are qualitatively similar to the two-dimensional case.

The similarity between two- and three-dimensional systems is one of the most relevant consequences of the presence of reflecting boundary. In fact, in the no boundary case, two and three dimensional problems were drastically different. Even though the MFET is infinite in both cases, the recurrent Brownian motion performs a compact exploration of space and visits any infinitesimal region with unit probability, whereas the transient diffusion in three dimensions may escape to infinity and never return, in which case encounter never happens. In contrast, the boundness of the domain with reflecting boundary makes diffusion recurrent in any dimension, while the MFET is always finite. This justifies the similar qualitative behavior in 2D and 3D. In the remainder of the section, we undertake a systematic analysis of the survival probability and of the FET probability density in 3D and compare them with their 2D counterparts.

As in the 2D case, we introduce two timescales t_B and t_F via Eqs. (67, 68). The survival probability remains very close to $S_{\text{free}}(t|\mathbf{x}_1, \mathbf{x}_2)$ up to t_B . This is confirmed by Fig. 12(a), which shows the survival probability for four different settings (see caption). At times around t_B , the survival probability for the case (iv) of a fixed target is lower than that for the case (iii) of diffusing particles, if the particles are located near the center of the sphere. In turn, if both diametrically opposed particles are far from the center, the case (ii) of diffusing particles favors rapid encounters as compared to the case (i) of a fixed target. The explanation is the same as in 2D, where a centered position of a fixed target helps to avoid large first-encounter times.

Figure 12(b) illustrates the exponential decay of the survival probability at long times. One can see that empty symbols corresponding to diffusing particles fol-

Case	Decay time		MFET	
	T (δT)	\bar{T}	\bar{T}	\bar{T}^*
(i)	21.2 (0.3)	25.4	25.4	
(ii)	16.9 (0.5)	20.8	20.8	
(iii)	16.9 (0.6)	13.2	13.2	
(iv)	9.5 (0.4)	8.5	8.5	

TABLE IV: The decay time T , estimated error δT , and two estimates \bar{T} and \bar{T}^* of the MFET from Eqs. (59, 66) for two spherical particles, initially placed at $(-r/2, 0, 0)$ and $(r/2, 0, 0)$ inside a ball of radius $R = 4$, with (i) $D_1 = 1$, $D_2 = 0$ and $r = 6$, (ii) $D_1 = D_2 = 1/2$ and $r = 6$, (iii) $D_1 = D_2 = 1/2$ and $r = 2$, and (iv) $D_1 = 1$, $D_2 = 0$ and $r = 2$. For comparison, the small-target asymptotic formula (51) yields $T \approx 9.9$ for the case (ii); in turn, this formula is not applicable for the case (iv) as the target is too close to the boundary. Note that $\rho/\bar{R} \approx 0.29$ is not small, which can explain discrepancies. At the same time, Eq. (71) with $C_3 = 1.2$ yields $T \approx 17.2$ for the cases (i) and (iii), which differs from the simulation results by less than 2%.

low two close parallel straight lines, confirming that the decay time T is independent of the initial positions. In turn, filled symbols corresponding to a fixed target follow straight lines with distinct slopes, highlighting the dependence of T on the target position.

Figure 12(c) shows the corresponding FET probability densities. Like in the 2D case, the timescales t_F and t_B determine their shapes. Here, $t_B \simeq 2.0$ for all cases. Cases (i) and (ii) present two humps, since $t_F \simeq 0.7 \ll t_B$. In contrast, for cases (iii) and (iv) $t_F \simeq 6 \gg t_B$ and the probability densities present a single hump. As T is independent on the initial positions of the particles in cases (ii) and (iii), the long-time decay of the probability density is roughly the same; in turn, it is different for cases (i) and (iv), for which T depends on the initial position of the target (see Table IV).

One important difference with respect to the two-dimensional case is the dependence of T on the size of the system. As in 2D, one might be led to think that Eq. (40), which was obtained for a fixed small target, is still valid for diffusing particles upon setting $D = D_1 + D_2$. Figure 13 shows the decay time T as a function of \bar{R}^3 for different values of \bar{R} for two sets of diffusion constants. In both cases, the scaling of T with \bar{R}^3 is confirmed,

$$T \simeq C_3 \frac{\bar{R}^3}{3D\rho}, \quad (71)$$

but, in contrast to the prefactor $C_2 \simeq 1$ for the two-dimensional case, here one has $C_3 \simeq 1.2$. This result reflects again the singular character of the limit $D_1/D_2 \rightarrow 0$.

VIII. CONCLUSIONS

In this paper, we studied the distribution of the first-encounter time for two particles diffusing in bounded do-

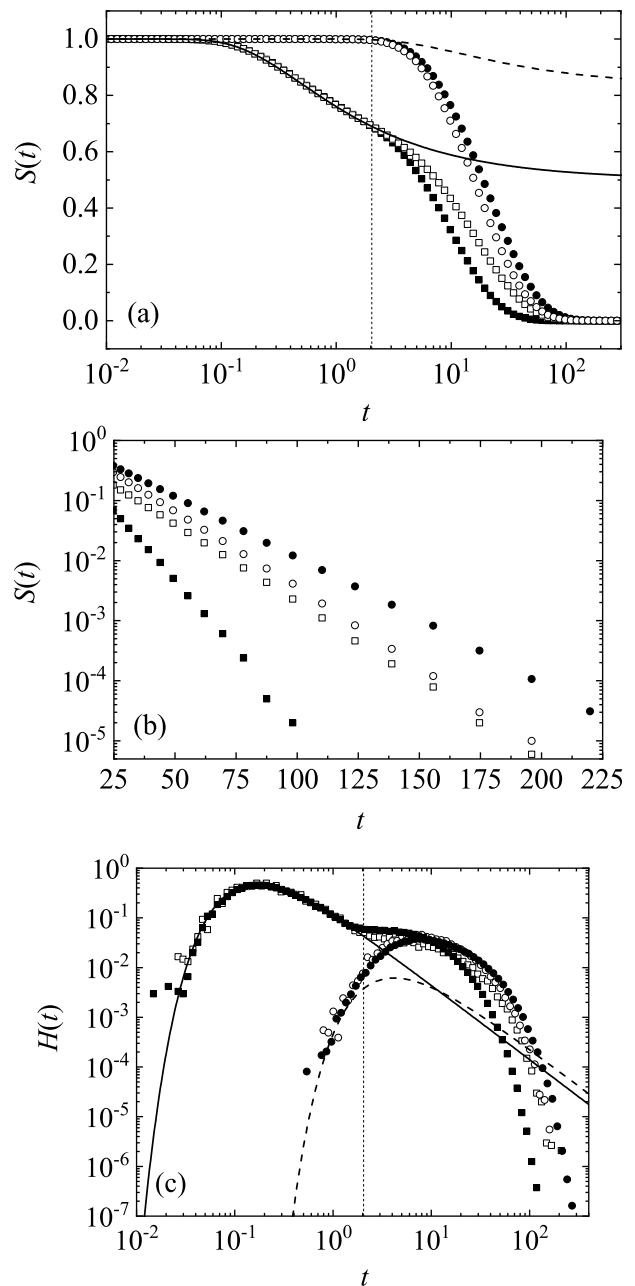


FIG. 12: (a,b) Survival probability for two diffusing particles initially located at $(-r/2, 0, 0)$ and $(r/2, 0, 0)$ inside a ball of radius $R = 4$. Four considered cases are: (i) $r = 6$, $D_1 = 1$ and $D_2 = 0$ (filled circles), (ii) $r = 6$, $D_1 = 1/2$ and $D_2 = 1/2$ (empty circles), (iii) $r = 2$, $D_1 = 1/2$ and $D_2 = 1/2$ (empty squares), and (iv) $r = 2$, $D_1 = 1$ and $D_2 = 0$ (filled squares). Lines show $S_{\text{free}}(t|\mathbf{x}_1, \mathbf{x}_2)$ given by Eq. (15) for $r = 6$ (dashed) and $r = 2$ (solid). Vertical dashed line indicates the value of $t_B = 2.0$. Panel (a) shows a linear-log plot, whilst the log-linear representation for long times is presented on panel (b). (c) FET probability density.

main with reflecting boundary. Even though this is a typical situation for many biochemical reactions, most former studies focused on the much simpler case with a

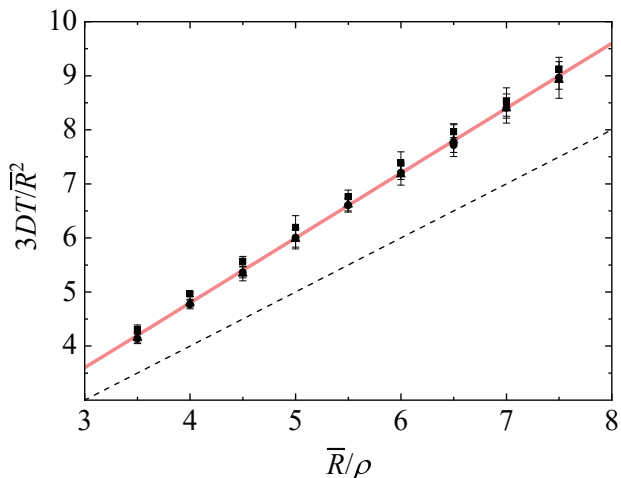


FIG. 13: Scaled decay time T versus the scaled effective radius \bar{R}/ρ for two diffusing particles started from positions $(-1, 0, 0)$ and $(1, 0, 0)$ inside a confining sphere of radius R equal to 4, 4.5, 5, 5.5, 6, 6.5, 7, 7.5, and 8, when $D_1 = 0.9$ and $D_2 = 0.1$ (squares), $D_1 = D_2 = 1/2$ (circles), and $D_1 = 1$ and $D_2 = 1/2$ (triangles). Solid and dashed lines correspond to Eq. (71) with $C_3 = 1.2$ and $C_3 = 1$, respectively.

fixed target ($D_2 = 0$). This problem of searching for a fixed target by a single diffusing particle was therefore a reference benchmark in our analysis, in spite of the singular character of the $D_2/D_1 \rightarrow 0$ limit. Another benchmark is the no boundary case, for which the survival probability $S_{\text{free}}(t|\mathbf{x}_1, \mathbf{x}_2)$ and the FET probability density $H_{\text{free}}(t|\mathbf{x}_1, \mathbf{x}_2)$ are known explicitly. The inclusion of a reflecting boundary significantly affects the survival probability and the FET distribution. In particular, the translational invariance of the no boundary case no longer holds. For instance, the reflecting boundary makes the survival probability and the FET distribution explicitly dependent on the initial positions of the particles with respect to the boundary, not only on the initial distance between the particles. This dependence is particularly significant at short times. Deviations from $S_{\text{free}}(t|\mathbf{x}_1, \mathbf{x}_2)$ are stronger when both particles are closer to the boundary.

We introduced two timescales, t_F and t_B , that qualitatively control the FET distribution. In particular, the survival probability and the FET probability density can be well approximated by $S_{\text{free}}(t|\mathbf{x}_1, \mathbf{x}_2)$ and $H_{\text{free}}(t|\mathbf{x}_1, \mathbf{x}_2)$ when $t \lesssim t_B$. In contrast, the confinement effect cannot be generally ignored at times exceeding t_B . In turn, the value of t_F determining the position of the maximum of $H_{\text{free}}(t|\mathbf{x}_1, \mathbf{x}_2)$, affects the shape of the FET probability density. When $t_F > t_B$, the FET probability density exhibits a single maximum and has a mildly broad shape. In turn, if $t_F \ll t_B$, the FET probability density is much broader, and a second hump can emerge at times of the order of t_B .

The third important timescale is the decay time T characterizing the long-time exponential decay of both

$S(t|\mathbf{x}_1, \mathbf{x}_2)$ and $H(t|\mathbf{x}_1, \mathbf{x}_2)$. If both particles are diffusing, the decay time T does not depend on the initial positions of the particles; in turn, if one particle is immobile (e.g., $D_2 = 0$), T depends on its fixed position. When the particles are small as compared to the confinement, our results suggest

$$T \simeq \frac{C_d \bar{R}^2}{Dd} \times \begin{cases} \ln(\bar{R}/\rho) & (d=2), \\ \bar{R}/\rho & (d=3), \end{cases} \quad (72)$$

where $D = D_1 + D_2$, $\bar{R} = R - \rho_1$ and $\rho = \rho_1 + \rho_2 = 2\rho_1$. The numerical prefactor C_2 was shown to be close to 1 in two dimensions, and $C_3 \approx 1.2$ in three dimensions. Explaining the deviation of C_3 from 1 remains an open problem. In the small-target limit, T is also close to the MFET.

Equation (72) can be related to the volume $v(T)$ of the Wiener sausage generated during time T by a diffusing particle with diffusion coefficient D and radius ρ [72]. As long as $DT/\rho^2 \gg 1$, it turns out that Eq. (72) with $C_d = 1$ provides the time T required by the diffusive particle to generate the volume of the Wiener sausage (i.e., the explored volume up to time T) equal to the volume $v(T)$ of the confining region of radius \bar{R} . This observation allows one to conjecture how the extension of (72) to $d > 3$ could look like: $T \simeq C_d \bar{R}^d / [d(d-2)D\rho^{d-2}]$, where we used the relation $v(T) = v_0 d(d-1)DT/\rho^2$ for $d \geq 3$ and DT/ρ^2 large, with v_0 being the volume of a d -dimensional sphere of unit radius [72].

The small- ρ behavior of T described by Eq. (72) is drastically different from that of the one-dimensional case. In the latter, there is no distinction between point-like and finite-size particles, i.e., the decay time is finite even at $\rho = 0$. Here, there is no small-target asymptotic relation like Eq. (72), and the dependence of the decay time T on the diffusion coefficients D_1 and D_2 is not reduced to that of $D_1 + D_2$ [64].

This work can be extended in several ways. First, for the sake of providing realistic descriptions, it is important to investigate the statistics of first-encounter times in biochemical reactions with reactants of different sizes. Even though the same simulation algorithms can be used, distinct radii add an extra length scale and thus make the introduction of timescales more subtle. Second, the effect of external forces that bias the random motion of diffusing particles can be important for biological and chemical applications. Third, one can consider particles undergoing subdiffusive dynamics, e.g., continuous-time random walks with heavy tailed waiting times [73, 74]. As the statistics of particle trajectories remains unchanged, the subordination concept suggests that exponential functions in the spectral decomposition of the survival probability will be replaced by Mittag-Leffler functions, allowing one to generalize our former results [17]. Similarly, one can consider diffusing diffusivity and switching diffusion models for the dynamics of both particles [23, 75, 76]. A rigorous mathematical analysis of the first-encounter distribution in the small target limit can further clarify

the important role of confinement in diffusion-influenced reactions. In particular, the derivation of the leading-order asymptotic relation (72) and the analysis of its dependence on the diffusion coefficients and the radii of the particles are still open.

Finally, one of the most important perspectives consists in accounting for partial reactivity of the particles. In fact, upon an encounter, the particles typically have to overcome an energy activation barrier or to undertake an appropriate conformational change in order to react. As a consequence, the reaction occurs with some probability which depends on the reactivity of the particles. The role of partial reactivity in the statistics of first-reaction times of a single particle diffusing towards a static target was thoroughly investigated [8, 16, 17, 24, 27, 35, 77, 78]. In particular, the concept of the boundary local time characterizing the number of encounters between the diffusing particle and the static target was put forward to describe the statistics of the first-reaction times [27, 79–83]. An extension of the current study to partially reactive particles and the associated statistics of encounters is of primary importance for a reliable description of bimolecular reactions.

Acknowledgments

F. L. V. acknowledges financial support by Junta de Extremadura (Spain) through Grants GR18079 and PD16010 (partially financed by FSE funds). S. B. Y. and E. A. acknowledge financial support from Grant PID2020-112936GB-I00 funded by MCIN/AEI/10.13039/501100011033, and from Grants IB20079, GR18079 and GR21014 funded by Junta de Extremadura (Spain) and by ERDF: A way of making Europe. D. S. G. acknowledges a partial financial support from the Alexander von Humboldt Foundation through a Bessel Research Award.

Appendix A: Appendix: Simulation procedure

In our algorithm, diffusing particles are modeled as continuous-time random walkers [73]. These particles move randomly by means of instantaneous jumps. The motion of each particle in a d -dimensional domain is determined by $d + 1$ random variables: waiting time of a particle until its next jump and its displacements along each of the d space directions. These random variables are drawn from corresponding waiting time and jump length distributions. In the algorithm, we fix the unit of time by setting the waiting time PDF to be the exponential distribution $\exp(-t)$. The random displacements carried out by the i th particle are drawn from zero-mean Gaussian distribution with variance σ_{ij}^2 , where $i = 1, 2$ for two particles, and $j = 1, \dots, d$. Therefore, the diffu-

sion coefficient of each particle is equal to

$$D_i = \frac{\sum_{j=1}^d \sigma_{ij}^2}{2d}. \quad (\text{A1})$$

To deal with isotropic diffusion, we choose $\sigma_{i1} = \dots = \sigma_{id}$ in all simulations. The use of the exponential and Gaussian PDFs is just a choice; other choices are possible but the waiting time density should have a finite mean, as well as the jump length PDF should have a finite variance to produce normal diffusion [74].

The structure of the program is the following. At the initial time, the centers of two particles are set in their prescribed initial positions. Then, the times at which the particles are expected to jump are assigned by means of an exponential random variable. The time in the simulation evolves until the minimum of both times. The particle with the smaller waiting time takes a jump, whereas the other particle remains at rest. The moving particle follows a straight line from its initial position to its destination.

In the no boundary case, only two simple situations could be distinguished. If the moving particle collides with the other particle, the simulation stops and the encounter time is recorded. Otherwise, the particle arrives at its destination and a new waiting time is assigned. The collision takes place if at least one of the following conditions is fulfilled: (i) the distance from the center of the static particle (that is, the particle momentarily at rest) to the destination is smaller than $\rho_1 + \rho_2$, where ρ_1 and ρ_2 denote respectively the radii of the moving and static particles; or (ii) there exists a region around the static particle inside the hypercylinder confined between the initial and final positions of the moving particle. Both situations are illustrated in Fig. 14 for two-dimensional systems (in this case, the aforementioned hypercylinder is just a rectangle).

However, in the case of bounded domains, the destination may be outside the confining domain. It is also possible that the destination is inside the domain, but its distance to the boundary is shorter than ρ_1 . For our purposes, both situations are equivalent, since the interaction of any particle of radius ρ_1 with a boundary of radius R is the same as that of a point-like particle with an effective boundary of radius $R - \rho_1$.

The implementation of the reflecting boundary can be done as follows. Let us assume that the moving particle travels a distance Δl in a single step, and that the center of the particle crosses the effective boundary of radius $R - \rho_1$ after traveling a distance δl . Let B be the point on the line of motion whose distance to the intersection is equal to $\Delta l - \delta l$, and assume that this point lies inside the effective disk. Loosely speaking, let us also term the radial direction as the line that joins the intersection with the center of the disk of radius $R - \rho_1$. Thus, the center of the moving particle after the jump is the point that is symmetric to B with respect to the radial direction. In this case, the encounter takes place provided that the

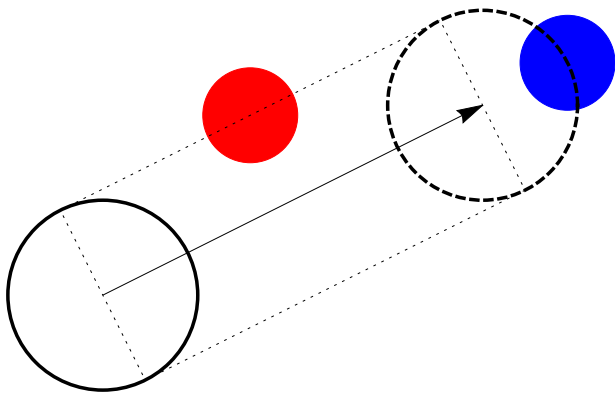


FIG. 14: Illustration of two possible encounters for a $2d$ system in the simulation algorithm. The empty disk shows the initial position of the moving particle, while the dashed circle would be its next location if there was no encounter. The arrow indicates the expected displacement of the center of the moving particle, whereas the rectangle delimited by dotted segments represents the area swept by the moving disk during its jump. The colored disks represent two possible positions of the static particle that will produce an encounter event.

moving particle collides with the static particle in the incoming trajectory, or after the reflection. Also, there is an encounter if the distance between the final position of the center of the moving particle and the center of the static particle is shorter than $\rho = \rho_1 + \rho_2$. Multiple reflections should be considered when the point B is outside the effective disk.

We also set a time cut-off in order to avoid very long trajectories prior to the encounter. The cut-off time is fixed at $t_{\text{cut}} = 2500$ for 2D systems and at $t_{\text{cut}} = 4000$ for 3D. In all cases, the number of realizations is $N = 10^6$.

Appendix B: Estimation of the decay time

Estimating the decay time from the long-time asymptotic behavior of the survival probability is not simple. As discussed in the main text, one should carefully select the range of times, (t_1, t_2) , over which the estimation is

performed. In fact, t should be long enough for the monoexponential decay to already have settled, and short enough to avoid statistical uncertainties and biases due to a limited number of Monte Carlo realizations. Figure 15 illustrates this point by showing the logarithmic derivative for 4 choices of D_1 (with $D_2 = 1 - D_1$), with the slower particle being at the center of the disk. For $D_1 = 0$ (fixed target), one observes a plateau for t from 250 to 500, and then a rapid decrease due to saturation artifacts. Using this range, one gets the estimate $T \approx 75$ given in Table III. Similarly, one gets accurate estimates of the decay time for $D_1 = 0.1$ and 0.5 . In contrast, the logarithmic derivative for the case $D_1 = 0.01$ does not exhibit a plateau, i.e., the exponential function $e^{-t/T}$ is

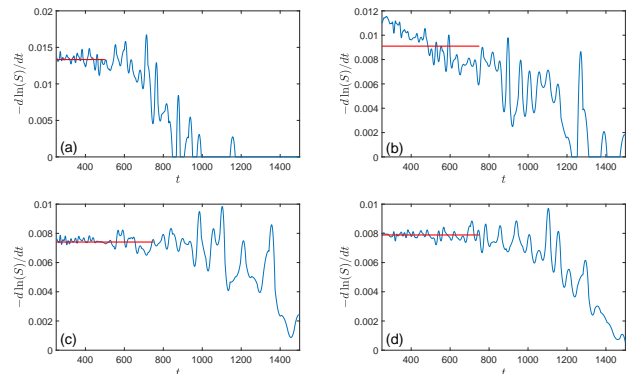


FIG. 15: The logarithmic derivative, $-d \ln S(t)/dt$, of the survival probability $S(t)$ for 4 choices of D_1 : 0 (a), 0.01 (b), 0.1 (c), and 0.5 (d), with $D_2 = 1 - D_1$. The first particle starts from the center of the disk of radius $R = 10$ and the second is located at $(5, 0)$. Horizontal red line indicates the range of times (t_1, t_2) used for estimating the decay time T . This estimation fails on the panel (b) because the monoexponential decay arises at longer times, at which the accuracy of simulations is too low.

affected by another slowly varying function on the considered range of times. One therefore needs a larger number of realizations or more efficient simulation methods (such as in [63]) to access the behavior of the survival probability at longer times, for which the monoexponential decay is well established.

[1] M. Smoluchowski, Versuch einer Mathematischen Theorie der Koagulations Kinetic Kolloider Lösungen, Z. Phys. Chem. **129**, 129-168 (1917).
 [2] S. Rice, *Diffusion-Limited Reactions* (Elsevier, Amsterdam, 1985).
 [3] D. A. Lauffenburger and J. Linderman, *Receptors: Models for Binding, Trafficking, and Signaling* (Oxford University Press, 1993).
 [4] S. Redner, *A Guide to First Passage Processes* (Cambridge: Cambridge University press, 2001).
 [5] Z. Schuss, *Brownian Dynamics at Boundaries and Inter-*

faces in Physics, Chemistry and Biology (Springer, New York, 2013).

[6] R. Metzler, G. Oshanin, and S. Redner (Eds.) *First-Passage Phenomena and Their Applications* (Singapore: World Scientific, 2014).
 [7] G. Oshanin, R. Metzler, K. Lindenberg (Eds.) *Chemical Kinetics: Beyond the Textbook* (New Jersey: World Scientific, 2019).
 [8] H. Sano and M. Tachiya, Partially diffusion-controlled recombination, J. Chem. Phys. **71**, 1276-1282 (1979).
 [9] N. Agmon and A. Szabo, Theory of reversible diffusion-

- influenced reactions, *J. Chem. Phys.* **92**, 5270 (1990).
- [10] P. Levitz, D. S. Grebenkov, M. Zinsmeister, K. Kolwankar, and B. Sapoval, Brownian flights over a fractal nest and first passage statistics on irregular surfaces, *Phys. Rev. Lett.* **96**, 180601 (2006).
- [11] S. Condamin, O. Bénichou, V. Tejedor, R. Voituriez, and J. Klafter, First-passage time in complex scale-invariant media, *Nature* **450**, 77 (2007).
- [12] S. Condamin, O. Bénichou, and M. Moreau, Random walks and Brownian motion: A method of computation for first-passage times and related quantities in confined geometries, *Phys. Rev. E* **75**, 021111 (2007).
- [13] D. S. Grebenkov, NMR Survey of Reflected Brownian Motion, *Rev. Mod. Phys.* **79**, 1077-1137 (2007).
- [14] O. Bénichou, D. S. Grebenkov, P. Levitz, C. Loverdo, and R. Voituriez, Optimal Reaction Time for Surface-Mediated Diffusion, *Phys. Rev. Lett.* **105**, 150606 (2010).
- [15] O. Bénichou, C. Chevalier, J. Klafter, B. Meyer, and R. Voituriez, Geometry-controlled kinetics, *Nature Chem.* **2**, 472-477 (2010).
- [16] D. S. Grebenkov, Searching for partially reactive sites: Analytical results for spherical targets, *J. Chem. Phys.* **132**, 034104 (2010).
- [17] D. S. Grebenkov, Subdiffusion in a bounded domain with a partially absorbing-reflecting boundary, *Phys. Rev. E* **81**, 021128 (2010).
- [18] O. Bénichou, C. Loverdo, M. Moreau, and R. Voituriez, Intermittent search strategies, *Rev. Mod. Phys.* **83**, 81-130 (2011).
- [19] P. C. Bressloff and J. M. Newby, Stochastic models of intracellular transport, *Rev. Mod. Phys.* **85**, 135-196 (2013).
- [20] O. Bénichou and R. Voituriez, From first-passage times of random walks in confinement to geometry-controlled kinetics, *Phys. Rep.* **539**, 225-284 (2014).
- [21] M. Galanti, D. Fanelli, S. D. Traytak, and F. Piazza, Theory of diffusion-influenced reactions in complex geometries, *Phys. Chem. Chem. Phys.* **18**, 15950-15954 (2016).
- [22] T. Guérin, N. Levernier, O. Bénichou, and R. Voituriez, Mean first-passage times of non-Markovian random walkers in confinement, *Nature* **534**, 356-359 (2016).
- [23] Y. Lanoiselée, N. Moutal, and D. S. Grebenkov, Diffusion-limited reactions in dynamic heterogeneous media, *Nat. Commun.* **9**, 4398 (2018).
- [24] D. S. Grebenkov, Spectral theory of imperfect diffusion-controlled reactions on heterogeneous catalytic surfaces, *J. Chem. Phys.* **151**, 104108 (2019).
- [25] D. S. Grebenkov and S. Traytak, Semi-analytical computation of Laplacian Green functions in three-dimensional domains with disconnected spherical boundaries, *J. Comput. Phys.* **379**, 91-117 (2019).
- [26] D. S. Grebenkov, Diffusion toward non-overlapping partially reactive spherical traps: fresh insights onto classic problems, *J. Chem. Phys.* **152**, 244108 (2020).
- [27] D. S. Grebenkov, Paradigm Shift in Diffusion-Mediated Surface Phenomena, *Phys. Rev. Lett.* **125**, 078102 (2020).
- [28] D. Holcman and Z. Schuss, Escape Through a Small Opening: Receptor Trafficking in a Synaptic Membrane, *J. Stat. Phys.* **117**, 975-1014 (2004).
- [29] Z. Schuss, A. Singer, and D. Holcman, The narrow escape problem for diffusion in cellular microdomains, *Proc. Nat. Acad. Sci. USA* **104**, 16098-16103 (2007).
- [30] O. Bénichou and R. Voituriez, Narrow-Escape Time Problem: Time Needed for a Particle to Exit a Confining Domain through a Small Window, *Phys. Rev. Lett.* **100**, 168105 (2008).
- [31] S. Pillay, M. J. Ward, A. Peirce, and T. Kolokolnikov, An Asymptotic Analysis of the Mean First Passage Time for Narrow Escape Problems: Part I: Two-Dimensional Domains, *SIAM Multi. Model. Simul.* **8**, 803-835 (2010).
- [32] A. F. Cheviakov, M. J. Ward, and R. Straube, An Asymptotic Analysis of the Mean First Passage Time for Narrow Escape Problems: Part II: The Sphere, *SIAM Multi. Model. Simul.* **8**, 836-870 (2010).
- [33] A. F. Cheviakov, A. S. Reimer, and M. J. Ward, Mathematical modeling and numerical computation of narrow escape problems, *Phys. Rev. E* **85**, 021131 (2012).
- [34] J.-F. Rupprecht, O. Bénichou, D. S. Grebenkov, and R. Voituriez, Exit time distribution in spherically symmetric two-dimensional domains, *J. Stat. Phys.* **158**, 192-230 (2015).
- [35] D. S. Grebenkov and G. Oshanin, Diffusive escape through a narrow opening: new insights into a classic problem, *Phys. Chem. Chem. Phys.* **19**, 2723-2739 (2017).
- [36] D. S. Grebenkov, R. Metzler, and G. Oshanin, Towards a full quantitative description of single-molecule reaction kinetics in biological cells, *Phys. Chem. Chem. Phys.* **20**, 16393-16401 (2018).
- [37] D. S. Grebenkov, R. Metzler, and G. Oshanin, Full distribution of first exit times in the narrow escape problem, *New J. Phys.* **21**, 122001 (2019).
- [38] D. Holcman and Z. Schuss, The Narrow Escape Problem, *SIAM Rev.* **56**, 213-257 (2014).
- [39] J. J. Kozak, *Chemical Reactions and Reaction Efficiency in Compartmentalized Systems*, in *Adv. Chem. Phys.*, vol. 115, pp. 245-406, edited by I. Prigogine and S. A. Rice (John Wiley & Sons, Inc., Hoboken, NJ, USA, 2000).
- [40] J. J. Kozak, C. Nicolis, and G. Nicolis, Efficiency of encounter-controlled reaction between diffusing reactants in a finite lattice, *J. Chem. Phys.* **113**, 8168 (2000).
- [41] C. Nicolis, John J. Kozak and G. Nicolis, Encounter-controlled reactions between interacting walkers in finite lattices: Complex kinetics and many-body effects, *J. Chem. Phys.* **115**, 663 (2001).
- [42] J. L. Bentz, J. J. Kozak, E. Abad, and G. Nicolis, Efficiency of encounter-controlled reaction between diffusing reactants in a finite lattice: topology and boundary effects, *Physica A* **326**, 55 (2003).
- [43] E. Abad, G. Nicolis, J. L. Bentz, and J. J. Kozak, Synchronous vs. asynchronous dynamics of diffusion-controlled reactions, *Physica A* **326**, 69 (2003).
- [44] E. Abad, First-passage method for the study of the efficiency of a two-channel reaction on a lattice, *Phys. Rev. E* **72**, 021107 (2005).
- [45] E. Abad and J. J. Kozak, Inverted regions induced by geometric constraints on a classical encounter-controlled binary reaction, *Physica A* **370**, 501 (2006).
- [46] M. Moreau, G. Oshanin, O. Bénichou, and M. Coppey, Pascal principle for diffusion-controlled trapping reactions, *Phys. Rev. E* **67**, 045104(R) (2003).
- [47] A. Szabo, R. Zwanzig, and N. Agmon, Diffusion-Controlled Reactions with Mobile Traps, *Phys. Rev. Lett.* **61**, 2496 (1988).
- [48] S. Redner and P. L. Krapivsky, Capture of the lamb: Diffusing predators seeking a diffusing prey, *Am. J. Phys.*

- 67**, 1277 (1999).
- [49] R. A. Blythe and A. J. Bray, Survival probability of a diffusing particle in the presence of Poisson-distributed mobile traps, *Phys. Rev. E* **67**, 041101 (2003).
- [50] A. J. Bray and K. Winkler, Vicious walkers in a potential, *J. Phys. A: Math. Gen.* **37**, 5493-5501 (2004).
- [51] S. Yuste, G. Oshanin, K. Lindenberg, O. Bénichou, and J. Klafter, Survival probability of a particle in a sea of mobile traps: A tale of tails, *Phys. Rev. E* **78**, 021105 (2008).
- [52] R. Borrego, E. Abad, and S. Yuste, Survival probability of a subdiffusive particle in a d -dimensional sea of mobile traps, *Phys. Rev. E* **80**, 061121 (2009).
- [53] G. Oshanin, O. Vasilyev, P. L. Krapivsky, and J. Klafter, Survival of an evasive prey, *Proc. Nat. Acad. Sci. USA* **106**, 13696-13701 (2009).
- [54] S. R. McGuffee and A. H. Elcock, Diffusion, Crowding and Protein Stability in a Dynamic Molecular Model of the Bacterial Cytoplasm, *PLoS Comput. Biol.* **6**, e1000694 (2010).
- [55] S. K. Ghosh, A. G. Cherstvy, D. S. Grebenkov, and R. Metzler, Anomalous, non-Gaussian tracer diffusion in heterogeneously crowded environments, *New J. Phys.* **18**, 013027 (2016).
- [56] N. Samanta and R. Chakrabarti, Tracer diffusion in a sea of polymers with binding zones - mobile vs. frozen traps, *Soft Matter* **12**, 8554 (2016).
- [57] A. Amitai, I. Kupka, and D. Holcman, Computation of the Mean First-Encounter Time Between the Ends of a Polymer Chain, *Phys. Rev. Lett.* **109**, 108302 (2012).
- [58] J. C. Tzou, S. Xie, and T. Kolokolnikov, First-passage times, mobile traps, and Hopf bifurcations, *Phys. Rev. E* **90**, 062138 (2014).
- [59] E. Agliari, A. Blumen, and D. Cassi, Slow encounters of particle pairs in branched structures, *Phys. Rev. E* **89**, 052147 (2014).
- [60] E. Agliari, D. Cassi, L. Cattivelli, and F. Sartori, Two-particle problem in comblike structures, *Phys. Rev. E* **93**, 052111 (2016).
- [61] J. Peng and E. Agliari, First encounters on combs, *Phys. Rev. E* **100**, 062310 (2019).
- [62] S. D. Lawley and C. E. Miles, Diffusive Search for Diffusing Targets with Fluctuating Diffusivity and Gating, *J. Nonlin. Sci.* **29**, 2955-2985 (2019).
- [63] I. Nayak, A. Nandi, and B. Das, Capture of a diffusive prey by multiple predators in confined space, *Phys. Rev. E* **102**, 062109 (2020).
- [64] F. Le Vot, S. B. Yuste, E. Abad, and D. S. Grebenkov, First-encounter time of two diffusing particles in confinement. *Phys. Rev. E* **102**, 032118 (2020).
- [65] C. W. Gardiner, *Handbook of stochastic methods for physics, chemistry and the natural sciences* (Berlin, Springer, 1985).
- [66] P. Levitz, M. Zinsmeister, P. Davidson, D. Constantin, and O. Poncelet, Intermittent Brownian dynamics over a rigid strand: Heavily tailed relocation statistics in a simple geometry, *Phys. Rev. E* **78**, 030102(R) (2008).
- [67] D. S. Grebenkov and J.-F. Rupprecht, The escape problem for mortal walkers, *J. Chem. Phys.* **146**, 084106 (2017).
- [68] D. S. Grebenkov, R. Metzler, and G. Oshanin, Strong defocusing of molecular reaction times results from an interplay of geometry and reaction control, *Commun. Chem.* **1**, 96 (2018).
- [69] T. Kolokolnikov, M. S. Titcombe, and M. J. Ward, Optimizing the Fundamental Neumann Eigenvalue for the Laplacian in a Domain with Small Traps, *Eur. J. Appl. Math.* **16**, 161 (2005).
- [70] A. F. Cheviakov and M. J. Ward, Optimizing the principal eigenvalue of the Laplacian in a sphere with interior traps, *Math. Computer Model.* **53**, 1394-1409 (2011).
- [71] T. Calandre, O. Bénichou, and R. Voituriez, Accelerating search kinetics by following boundaries, *Phys. Rev. Lett.* **112**, 230601 (2014).
- [72] A. M. Berezhkovskii, Yu. A. Makhnovskii, and R. A. Suris, Wiener sausage volume moments, *J. Stat. Phys.* **57**, 333-346 (1989).
- [73] E. W. Montroll and G. H. Weiss, Random walks on lattices. II, *J. Math. Phys.* **6**, 167 (1965).
- [74] R. Metzler and J. Klafter, The random walk's guide to anomalous diffusion: A fractional dynamics approach, *Phys. Rep.* **339**, 1 (2000).
- [75] A. V. Chechkin, F. Seno, R. Metzler, and I. M. Sokolov, Brownian yet Non-Gaussian Diffusion: From Superstatistics to Subordination of Diffusing Diffusivities, *Phys. Rev. X* **7**, 021002 (2017).
- [76] D. S. Grebenkov, A unifying approach to first-passage time distributions in diffusing diffusivity and switching diffusion models, *J. Phys. A* **52**, 174001 (2019).
- [77] F. C. Collins and G. E. Kimball, Diffusion-controlled reaction rates, *J. Coll. Sci.* **4**, 425 (1949).
- [78] B. Sapoval, General Formulation of Laplacian Transfer Across Irregular Surfaces, *Phys. Rev. Lett.* **73**, 3314 (1994).
- [79] D. S. Grebenkov, Probability distribution of the boundary local time of reflected Brownian motion in Euclidean domains, *Phys. Rev. E* **100**, 062110 (2019).
- [80] D. S. Grebenkov, Surface Hopping Propagator: An Alternative Approach to Diffusion-Influenced Reactions, *Phys. Rev. E* **102**, 032125 (2020).
- [81] D. S. Grebenkov, Joint distribution of multiple boundary local times and related first-passage time problems with multiple targets, *J. Stat. Mech.* 103205 (2020).
- [82] D. S. Grebenkov, Statistics of boundary encounters by a particle diffusing outside a compact planar domain, *J. Phys. A: Math. Theor.* **54**, 015003 (2021).
- [83] D. S. Grebenkov, An encounter-based approach for restricted diffusion with a gradient drift. *J. Phys. A: Math. Theor.* **55**, 045203 (2022).